SAR application summary

- Production of surface displacement field maps:
  - Earthquakes (co-seismic)
  - Inter-seismic loading on faults
  - Landslides
  - Volcanoes
  - *Subsidence in urban areas*
- DEM production
- Detection of surface changes
  - Estimation of post-event damages
  - Mapping of eruptive deposits

DEM formation

Repeat-path interferometry

- Using 2 images acquired at different times (you need a large perp. Baseline) (monostatic interferograms)

$$-(\Phi_M - \Phi_S) = \Delta\Phi = \Delta\Phi_{spatial}(B_{perp}, z) + \Delta\phi_{atmo} + (4\pi/\lambda)\, d + \Delta\Phi_{noise}$$

$$\phi_{topo} \approx W\left\{\frac{-4\pi B_{\perp} h}{\lambda R \sin\theta}\right\}, \qquad \phi_{topo} \approx W\left\{\frac{-2\pi h}{h_a}\right\}.$$

- Using a time series

Single-path interferometry: using 2 images acquired at the same time (bistatic interferograms)
Advantage: a good coherence + No atmospheric problems

SRTM shuttle mission

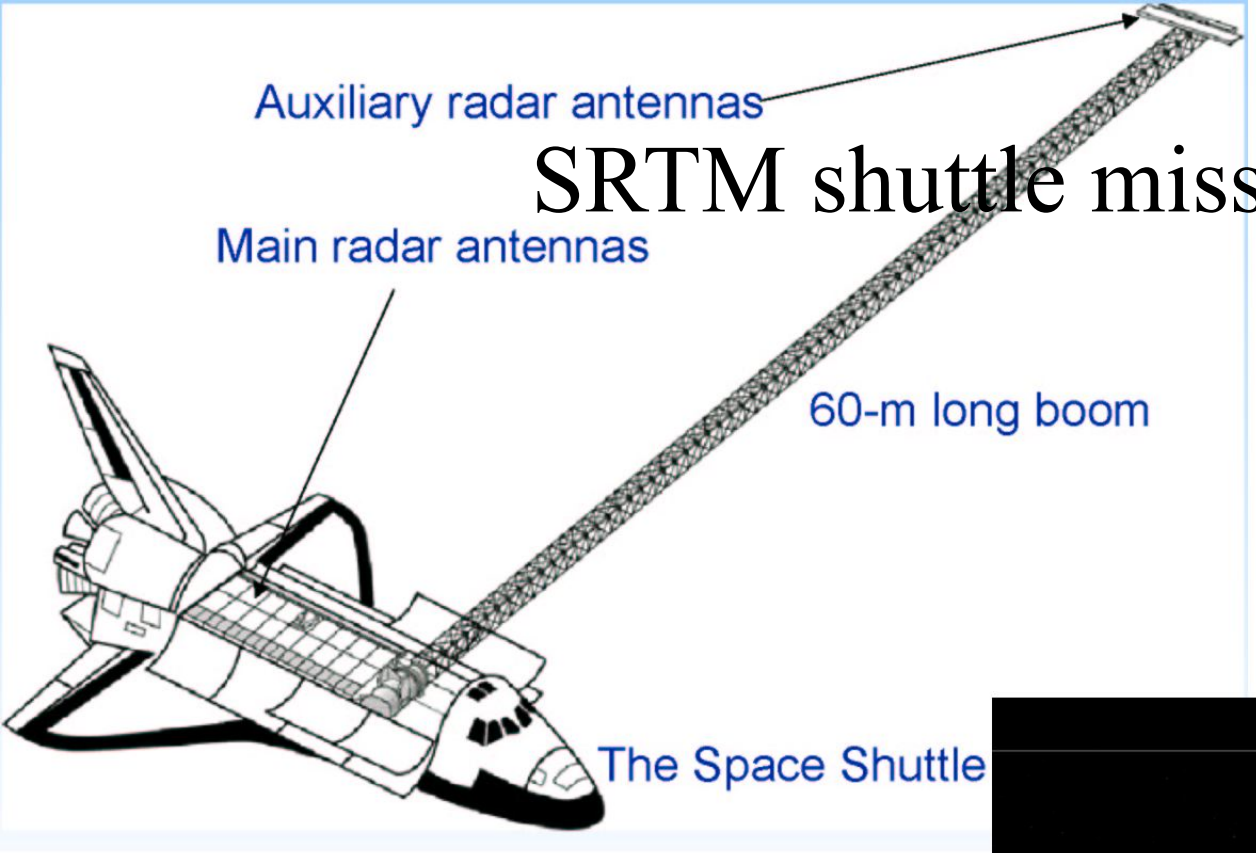

The MAST
60 m fixed baseline

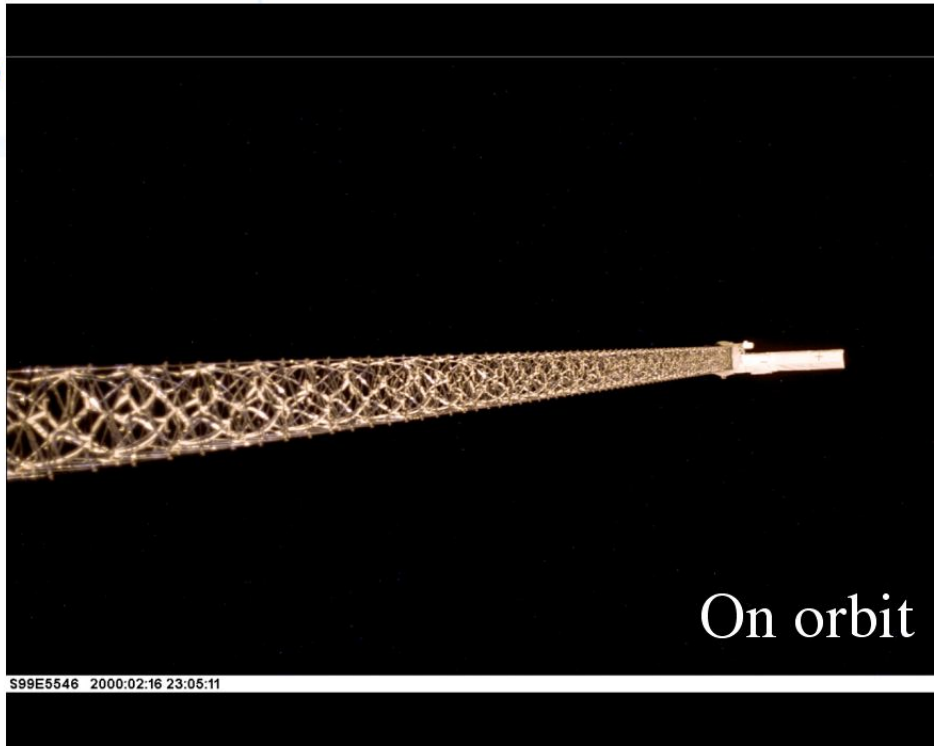

TanDEM-X

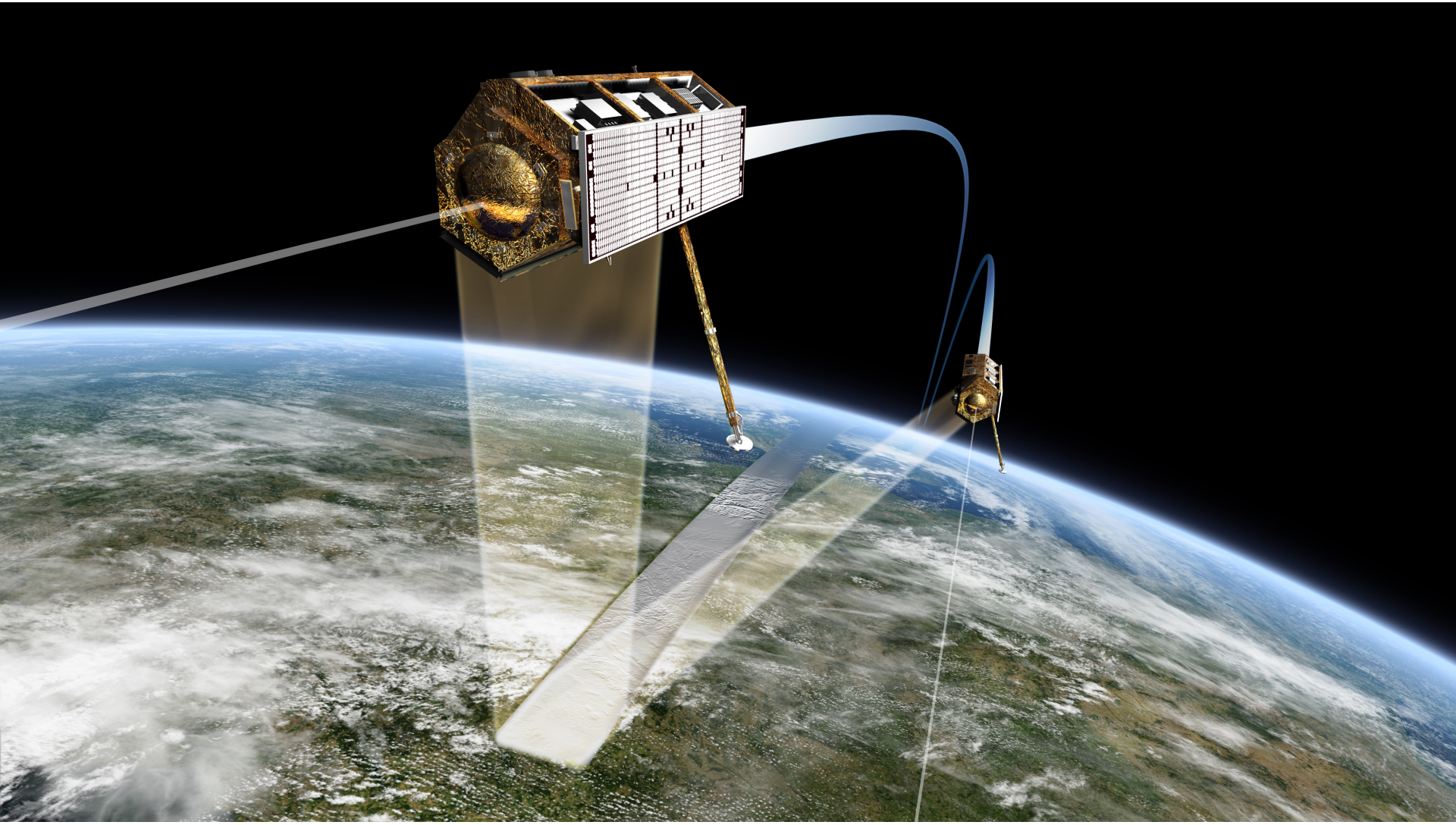

TanDEM-X

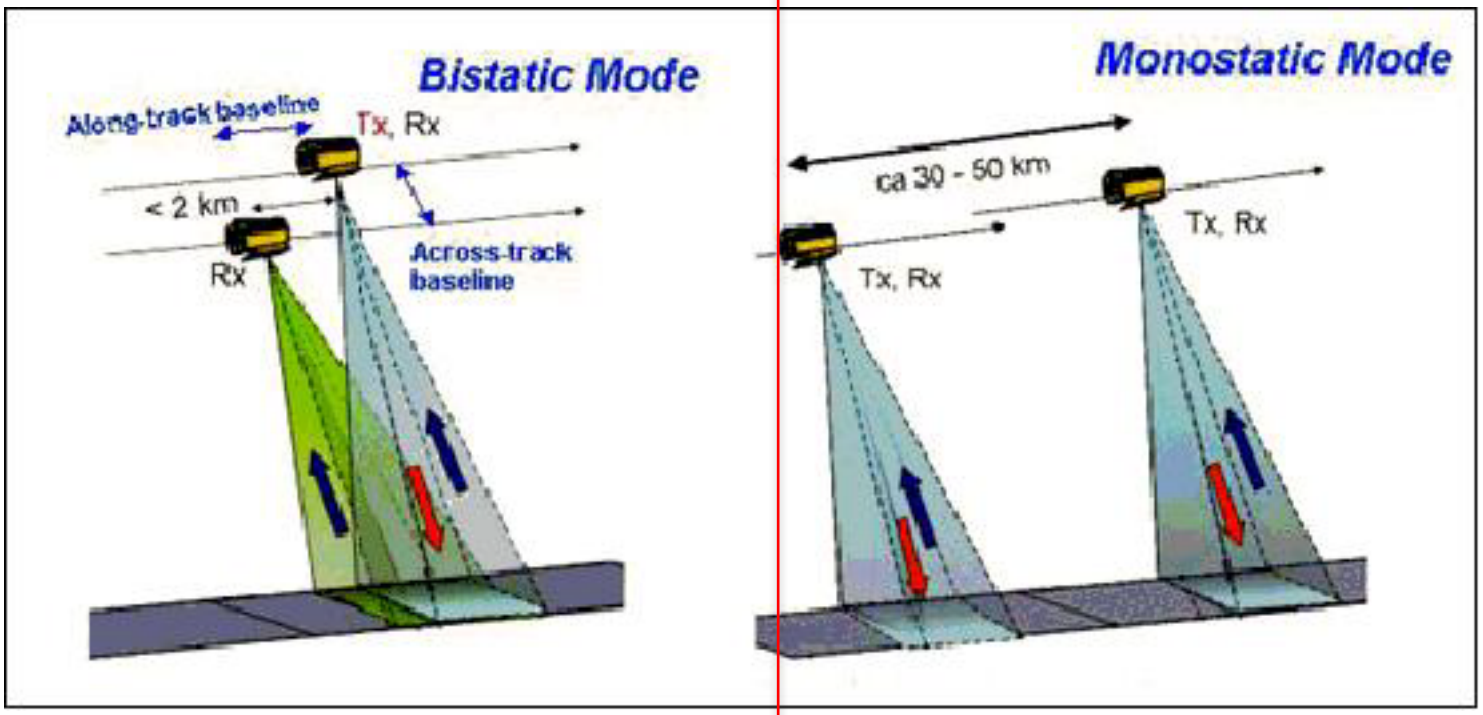
Bistatic Mode
Along-track baseline
Tx, Rx
< 2 km
Rx
Across-track baseline
Monostatic Mode
ca 30 - 50 km
Tx, Rx
Tx, Rx

TanDEM-X

Pink: 12m
Blue: 30m

Proposal DEM_GEOL1315 approved but only 5 tiles at 12m
And 5 tiles at 30m

TanDEM-X

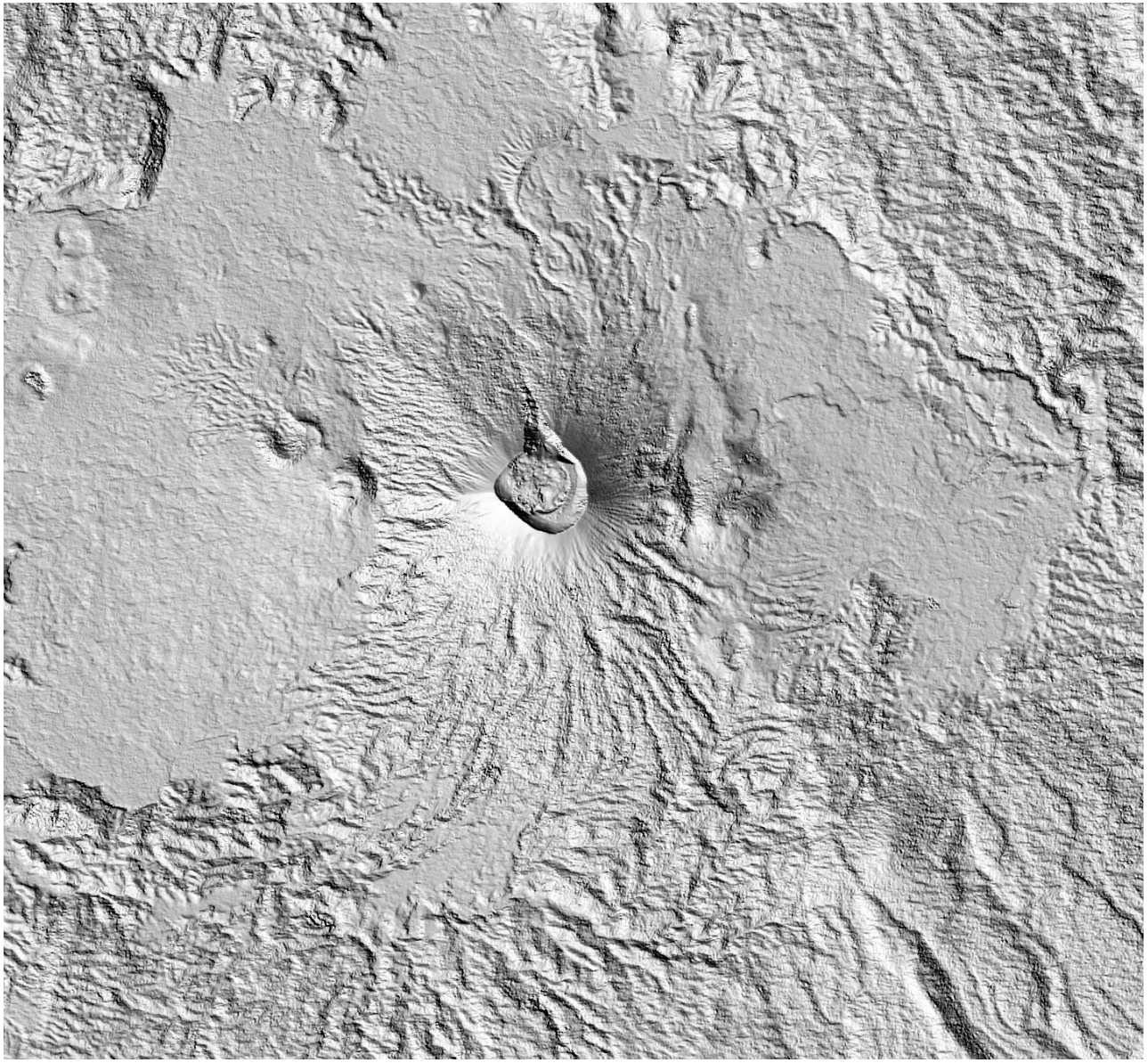

Ibu volcano

12.5m resolution

Images acquired between Dec 2010 and 2014

TanDEM-X

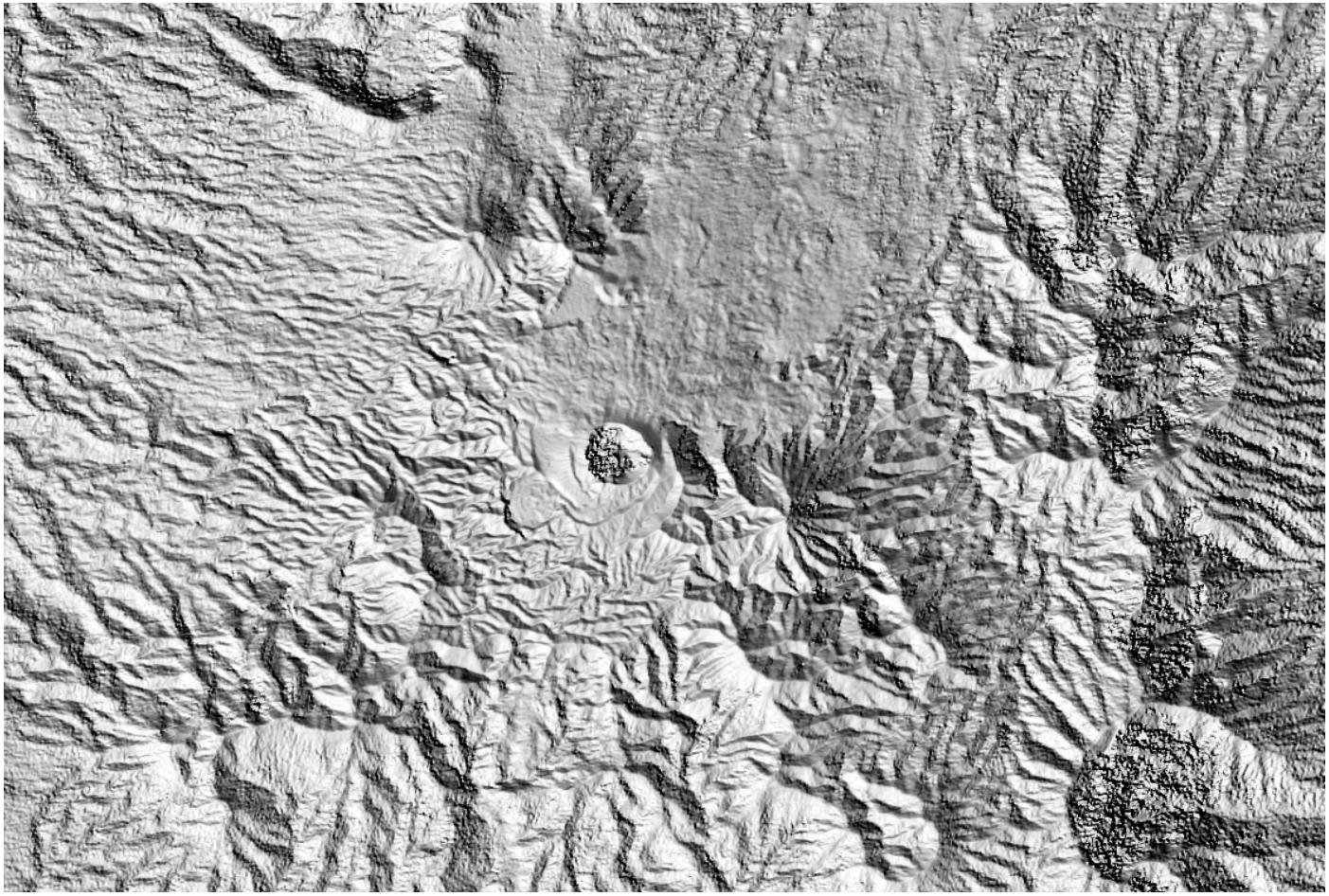

Dukono volcano

12.5m resolution

DEM formation

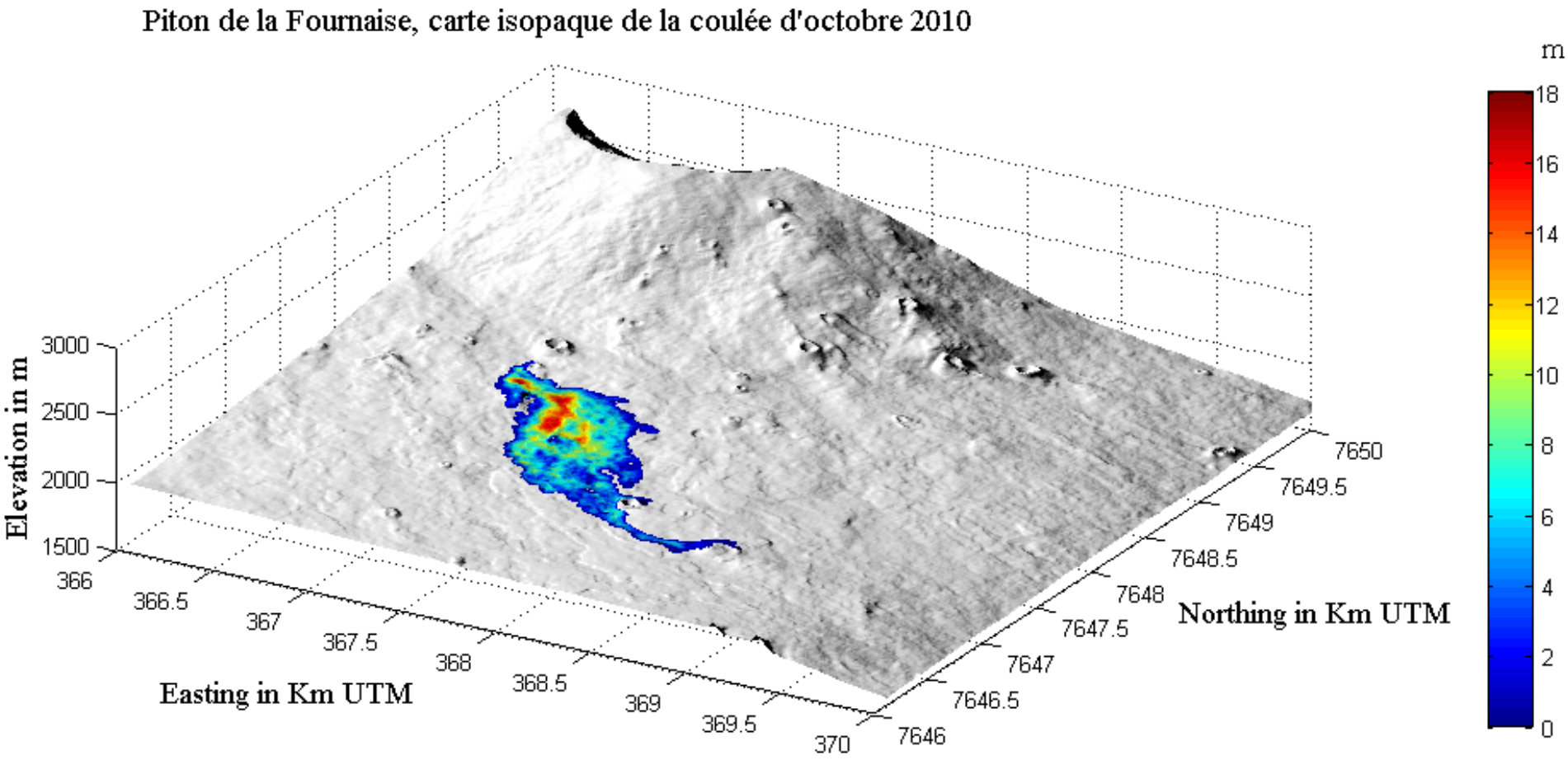

2010 lava thickness at Piton de la Fournaise obtained by single path interferometry Tandem-X data

Topography evolution➔ estimation of magma emission rate

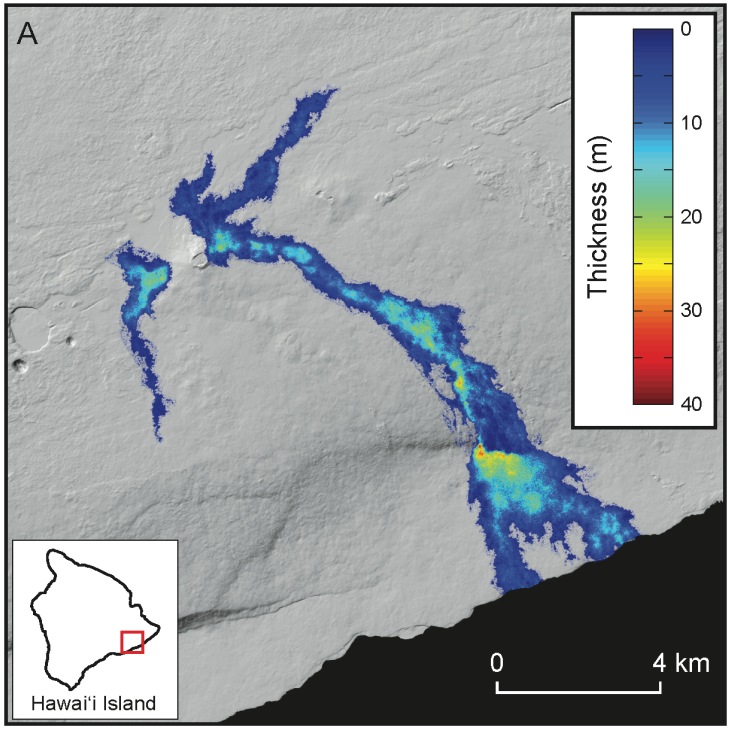

$$\phi_{topo} \approx W\left\{\frac{-4\pi B_{\perp} h}{\lambda R sin\theta}\right\},$$

Poland, 2014

Topography evolution➔ estimation of magma emission rate

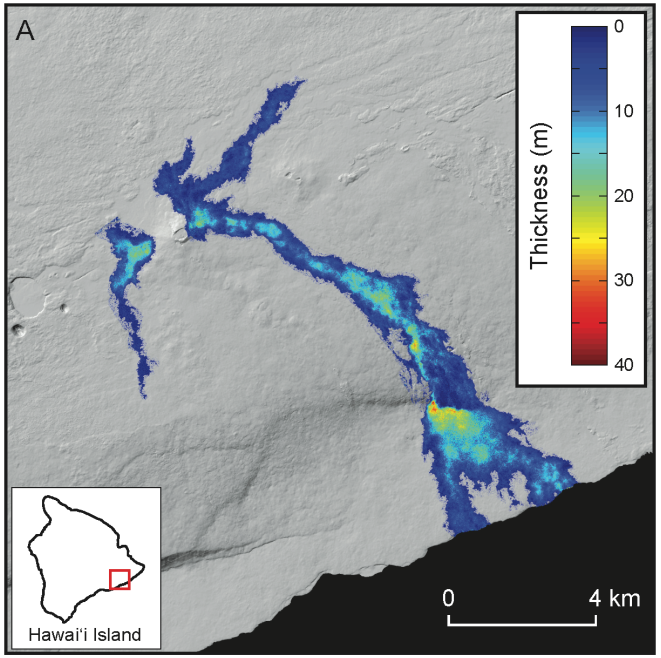

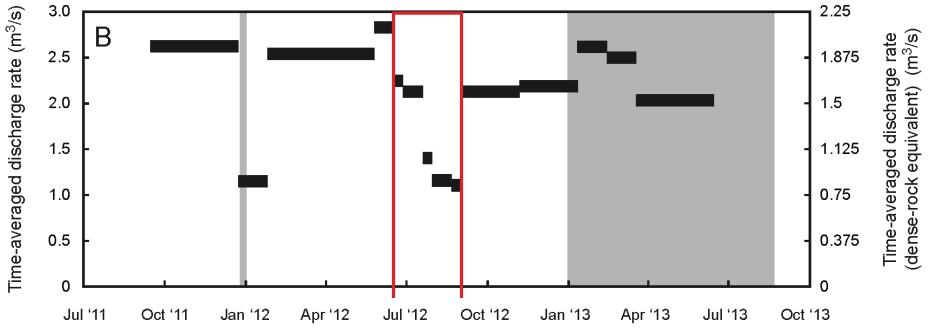

Poland, 2014

Information of the volcanic edifice growth…

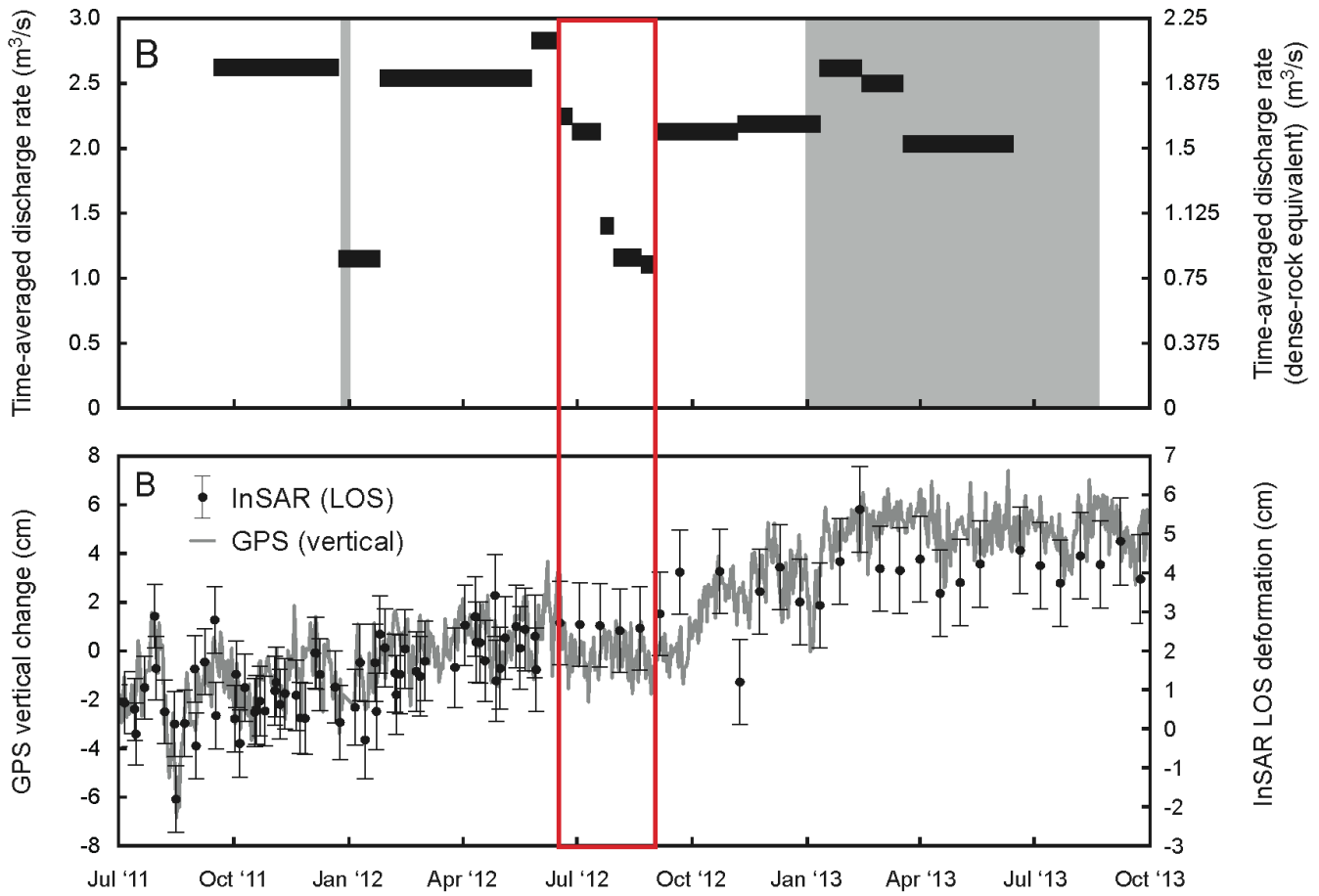

Poland, 2014

SAR application summary

- Production of surface displacement field maps:
  - Earthquakes (co-seismic)
  - Inter-seismic loading on faults
  - Landslides
  - Volcanoes
  - *Subsidence in urban areas*
- DEM production
- Detection of surface changes
  - Estimation of post-event damages
  - Mapping of eruptive deposits

How?

Amplitude

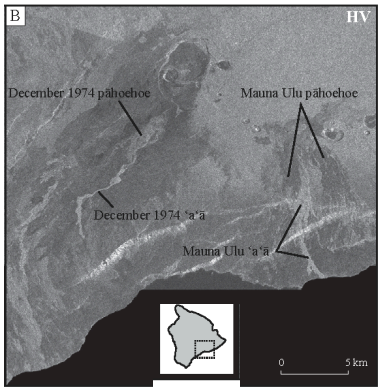

Pinel et al., 2014

Coherence (phase)

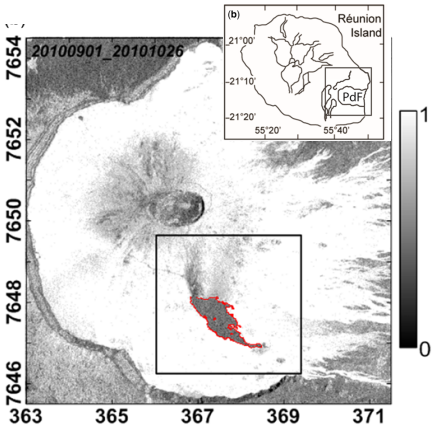

$$\rho = \frac{E[z_1 z_2^*]}{\sqrt{E[|z_1|^2]\ E[|z_2|^2]}},$$

Bato et al., 2010

SAR application summary

- Production of surface displacement field maps:
  - Earthquakes (co-seismic)
  - Inter-seismic loading on faults
  - Landslides
  - Volcanoes
  - *Subsidence in urban areas*
- DEM production
- Detection of surface changes
  - Estimation of post-event damages
  - Mapping of eruptive deposits

Estimation of post-event damages

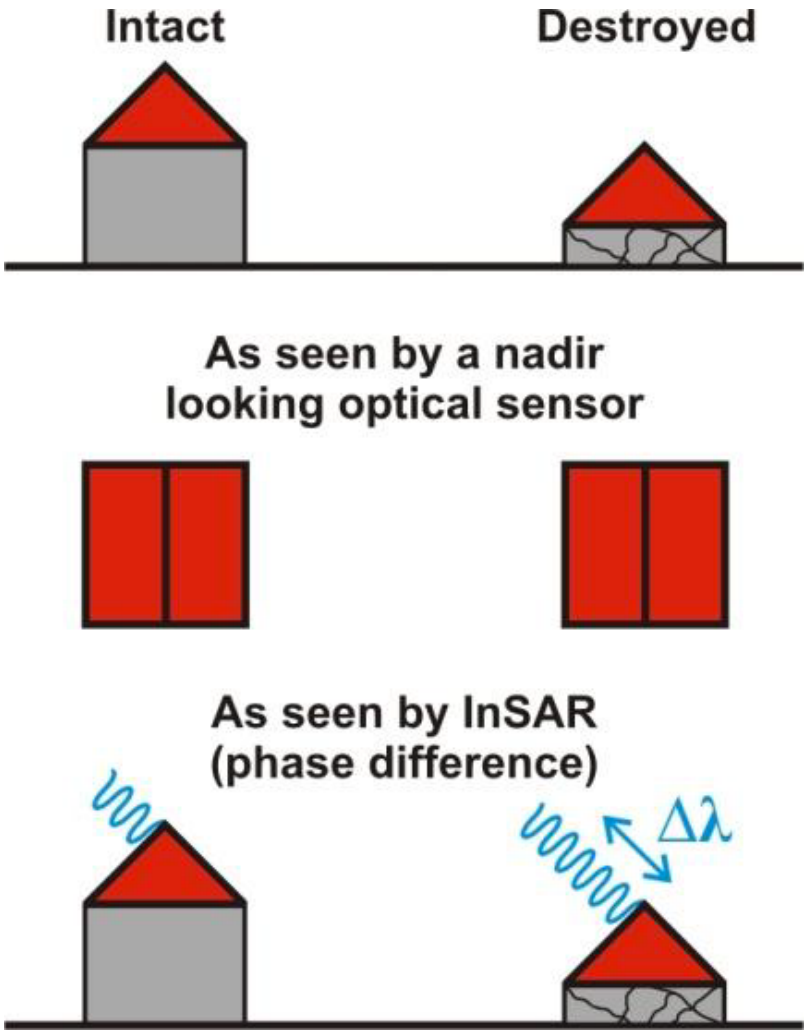

From Plank, 2014

Estimation of post-event damages

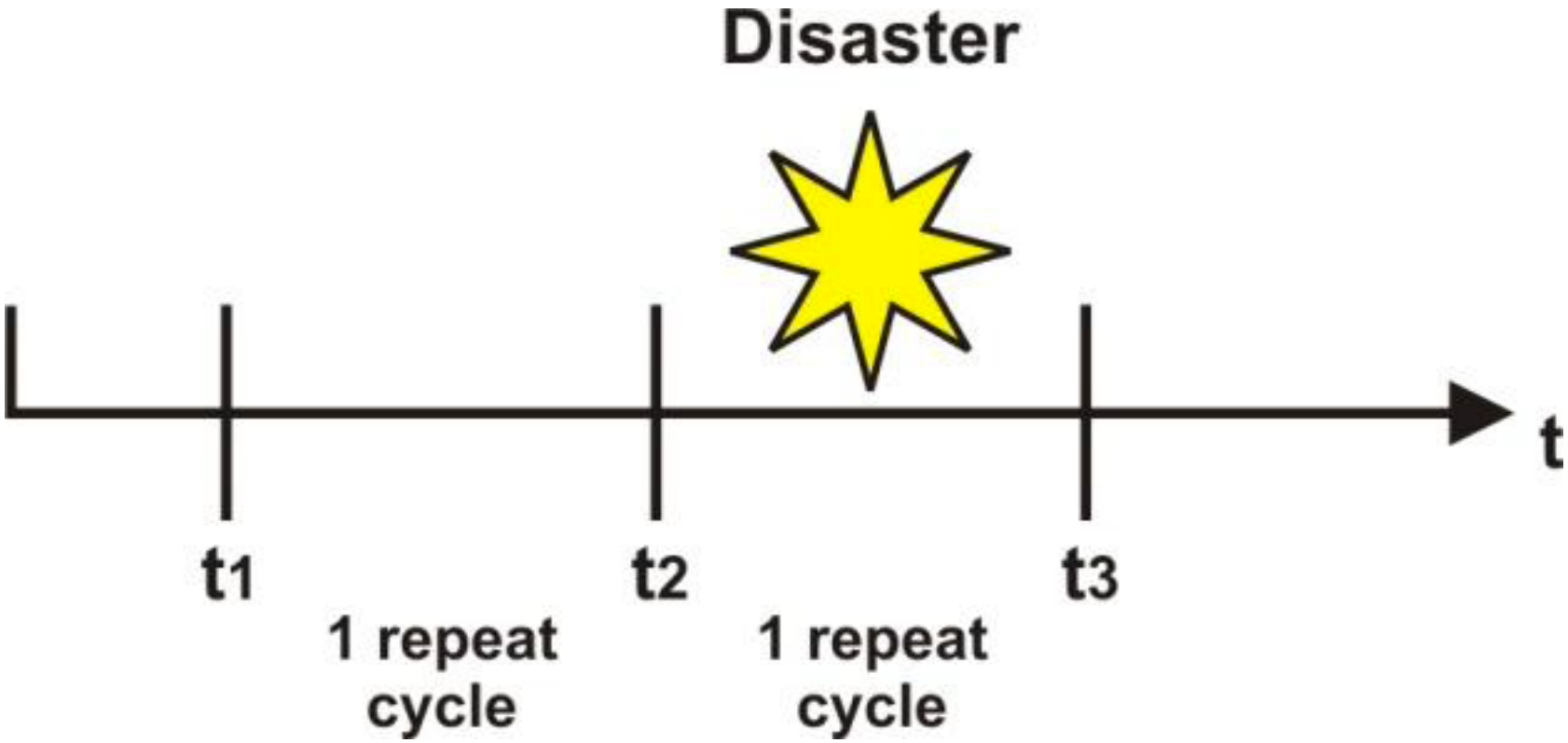

From Plank, 2014

Estimation of post-event damages

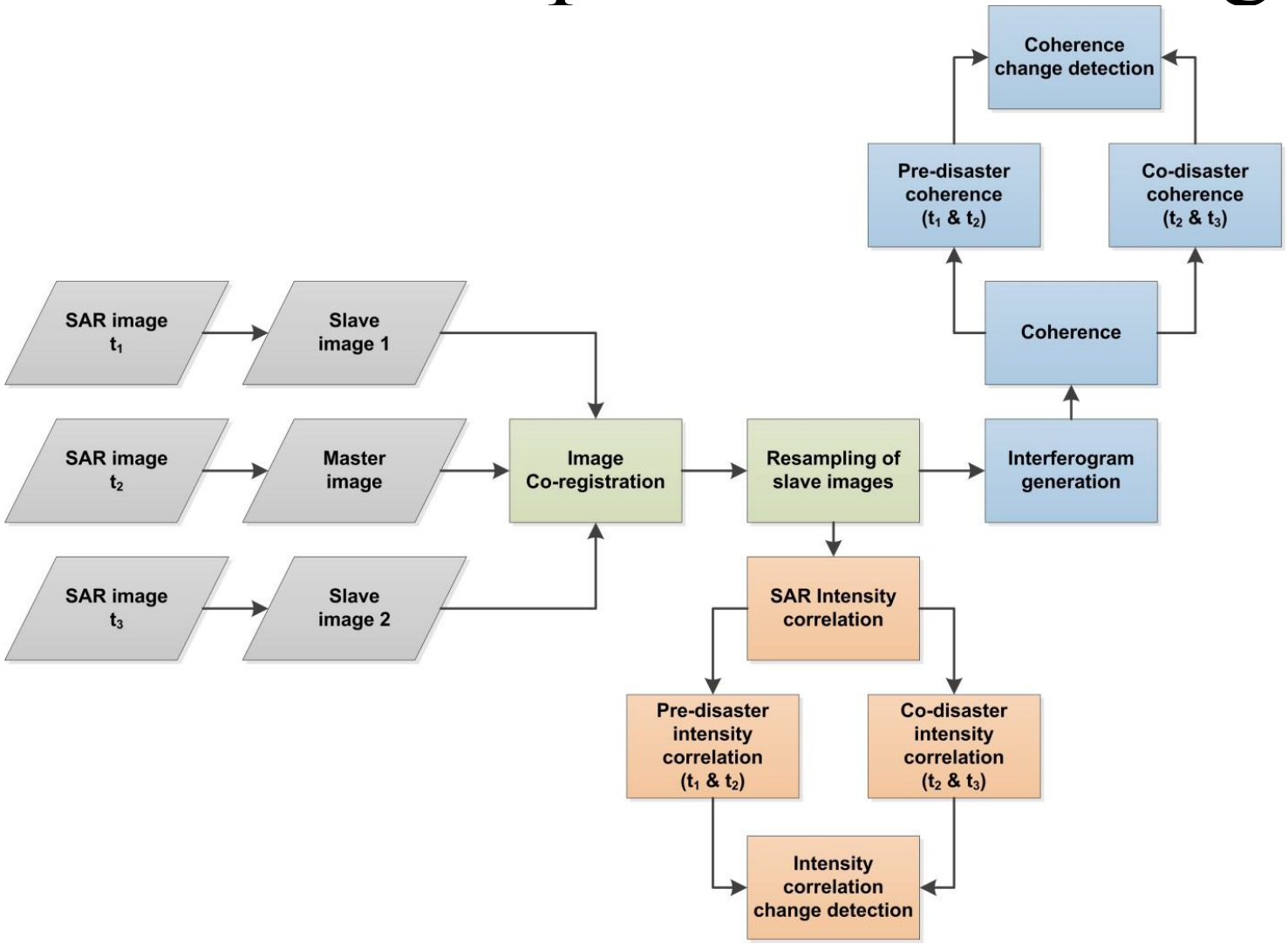

From Plank, 2014

Estimation of post-event damages

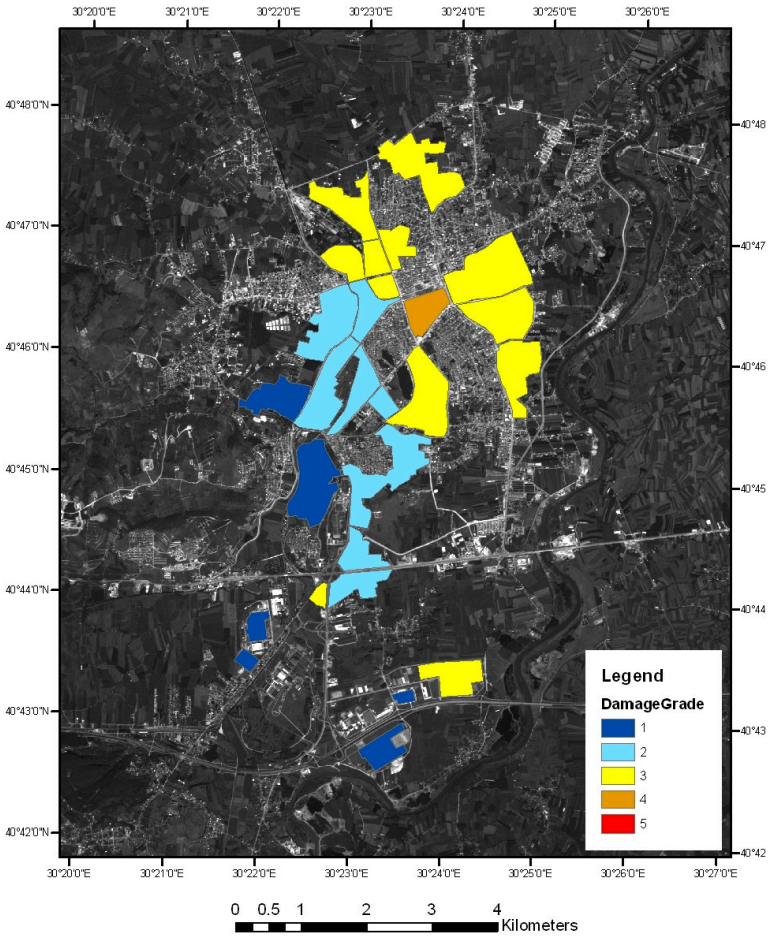

From Stramondo, et al.

SAR application summary

- Production of surface displacement field maps:
  - Earthquakes (co-seismic)
  - Inter-seismic loading on faults
  - Landslides
  - Volcanoes
  - *Subsidence in urban areas*
- DEM production
- Detection of surface changes
  - Estimation of post-event damages
  - Mapping of eruptive deposits

SAR data essential in volcanology for:

- Surface displacements quantification
- Topography evolution quantification
- Surface deposits mapping

Why is it important to efficiently map surface deposits?

- To produce hazard maps
- To validate numerical models for lava or pyroclastic flows
- To estimate magma eruptive volume and rate
- For lahar assessment

For lahar assessment

How to map?

Amplitude

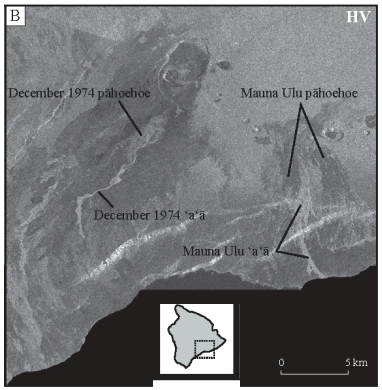

Pinel et al., 2014

Coherence (phase)

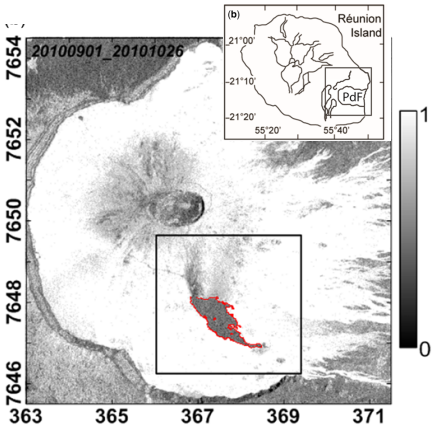

$$\rho = \frac{E[z_1 z_2^*]}{\sqrt{E[|z_1|^2]\ E[|z_2|^2]}},$$

Bato et al., 2010
Poster Froger et al

Most of the studies on basaltic volcanoes with effusive lava flows.
Less studies on andesitic/explosive volcanoes : Montserrat (Wadge et al, 2011), Unzen (Tenumura, 2005)….

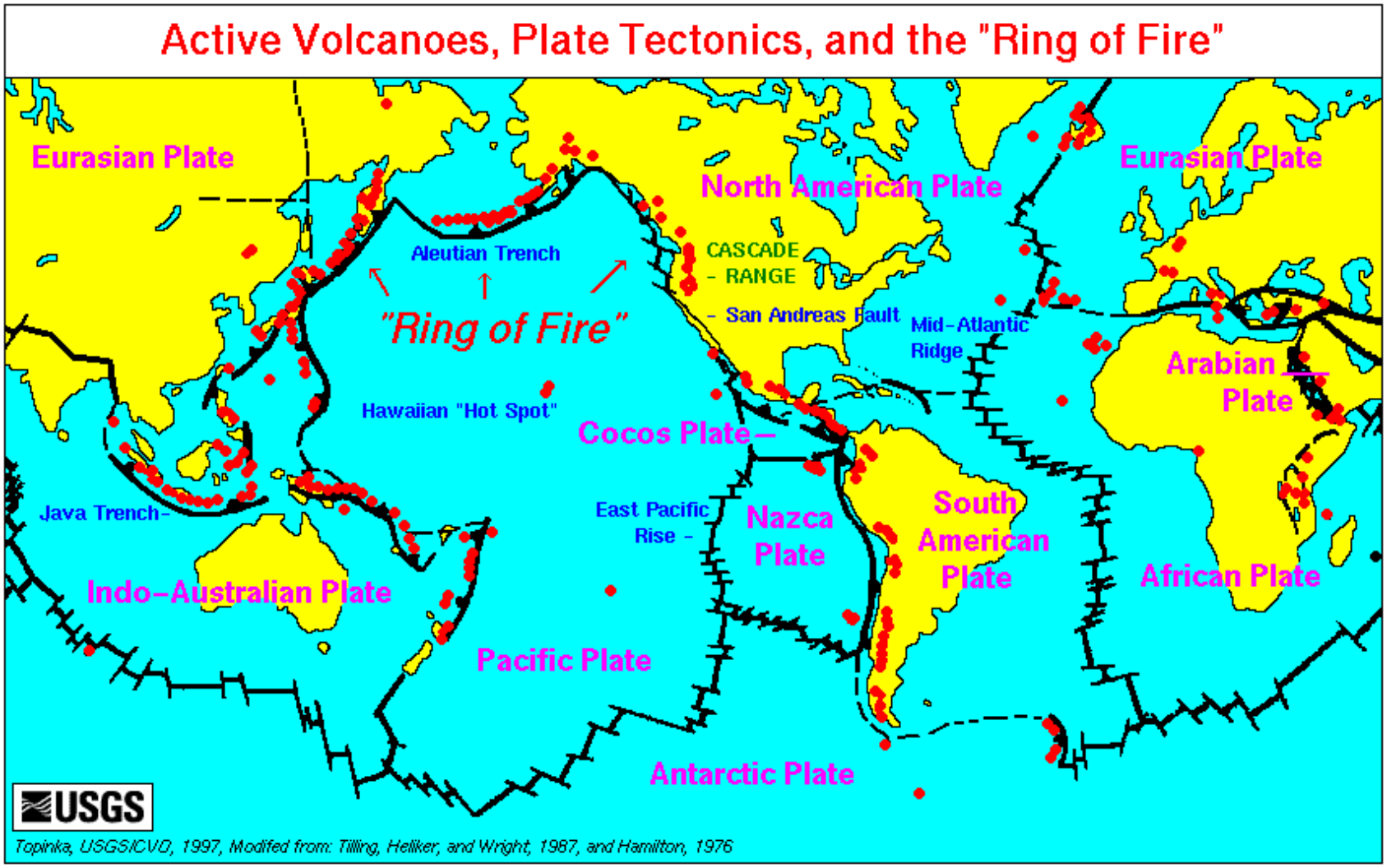
Active Volcanoes, Plate Tectonics, and the "Ring of Fire"
Eurasian Plate
North American Plate
Eurasian Plate
Aleutian Trench
CASCADE
- RANGE
- San Andreas Fault
"Ring of Fire"
Mid-Atlantic
Ridge
Arabian
Plate
Hawaiian "Hot Spot"
Cocos Plate
Java Trench
East Pacific
Rise
Nazca
Plate
South
American
Plate
African Plate
Indo-Australian Plate
Pacific Plate
Antarctic Plate
USGS
Topinka, USGS/CVO, 1997, Modified from: Tilling, Heliker, and Wright, 1987, and Hamilton, 1976

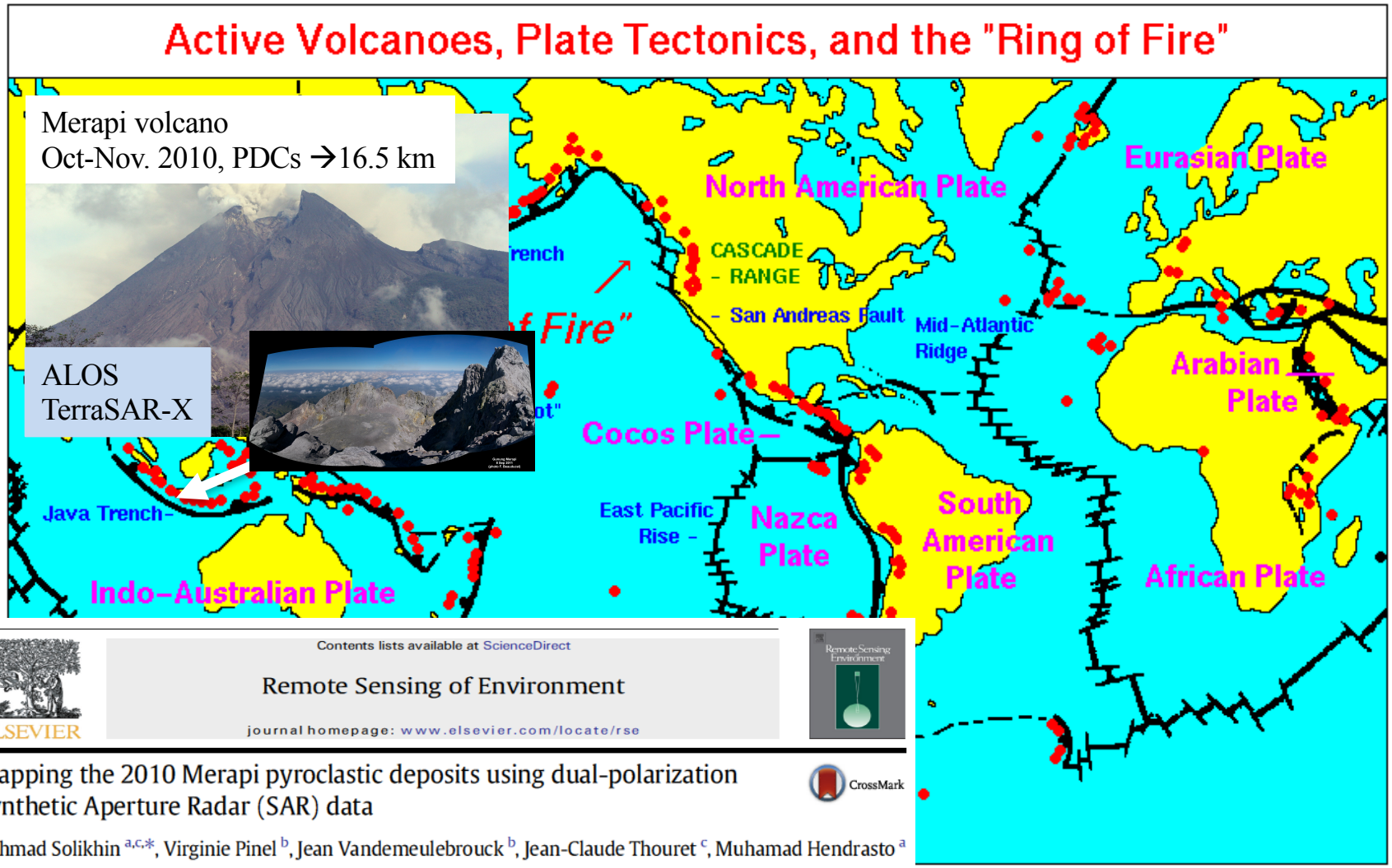

Contents lists available at ScienceDirect

Remote Sensing of Environment

journal homepage: www.elsevier.com/locate/rse

Mapping the 2010 Merapi pyroclastic deposits using dual-polarization Synthetic Aperture Radar (SAR) data

Akhmad Solikhin [a,c,*], Virginie Pinel [b], Jean Vandemeulebrouck [b], Jean-Claude Thouret [c], Muhamad Hendrasto [a]

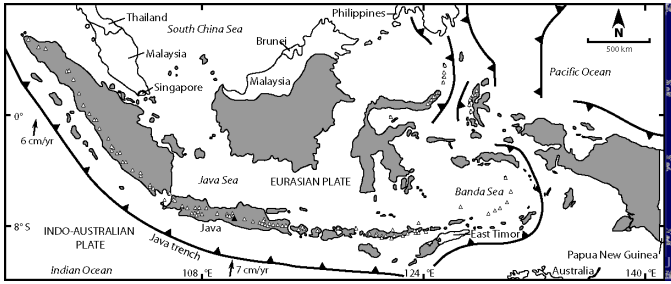

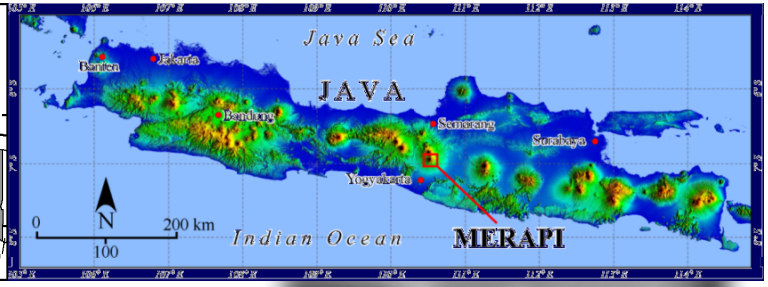

Merapi Hazard Map (Sayudi, et al., 2010)

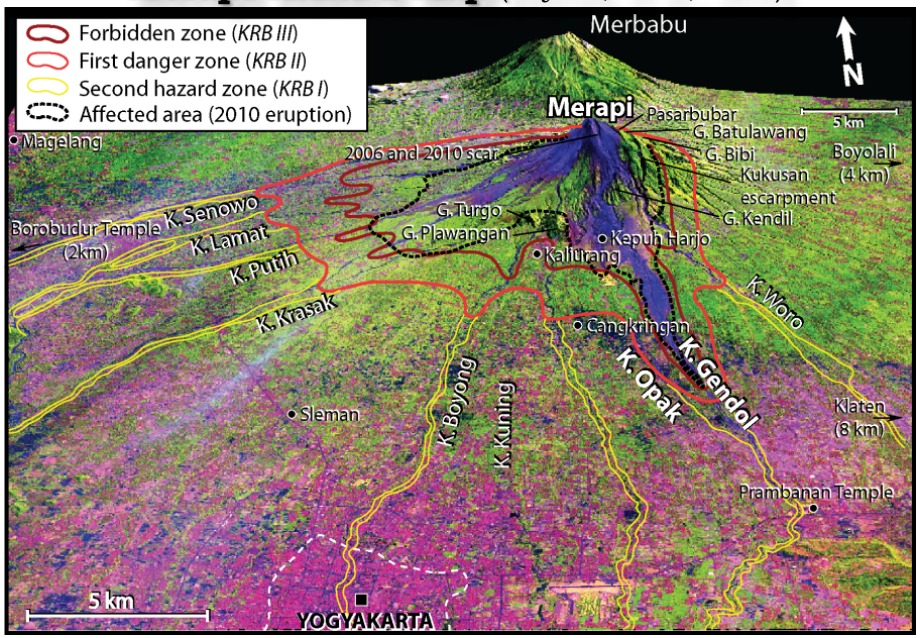

- **> 227,000 people live in the hazardous area**
- **Dome growth and collapse**
- **One eruption every 3 - 6 years**
- **VEI4 in 2010: largest over 145 years**
- **Several episodes of PDCs reaching 16.5 km from the summit**
- **Area covered: 22.3km^2**

The 2010 eruption (26 Oct.–23 Nov.)

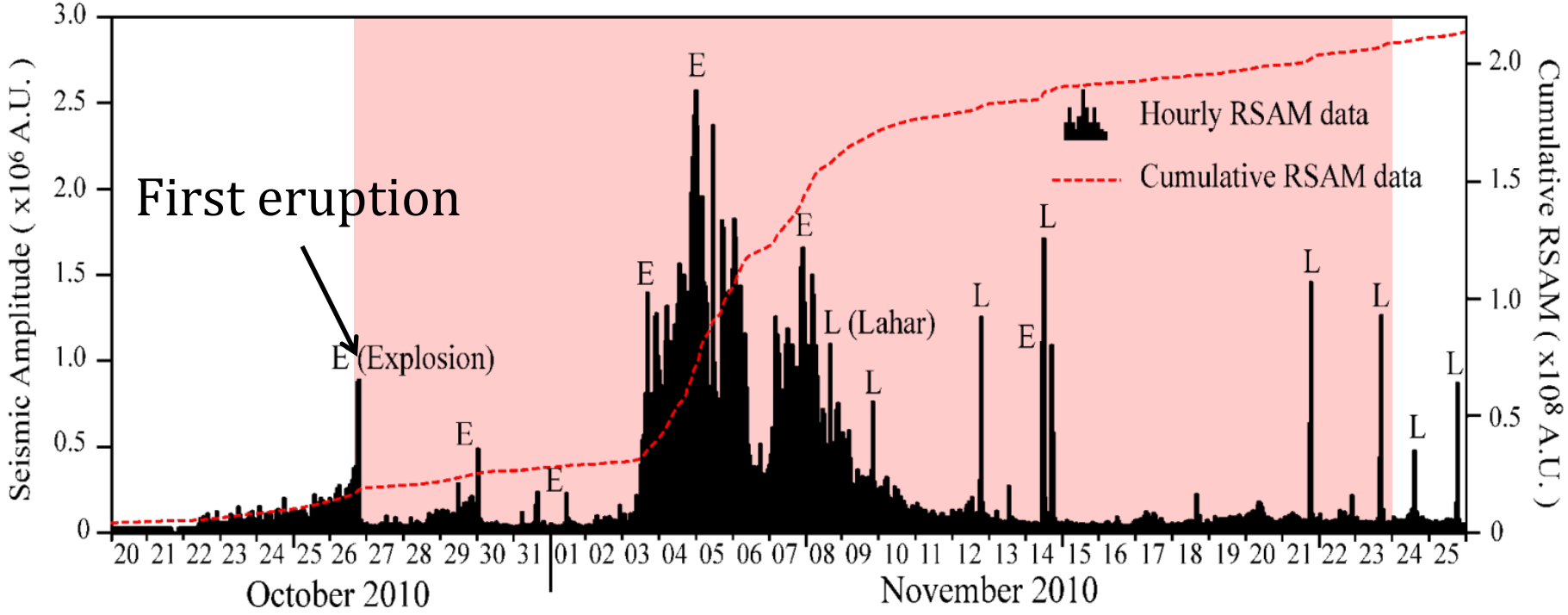

Real-time Seismic Amplitude Measurement (RSAM)

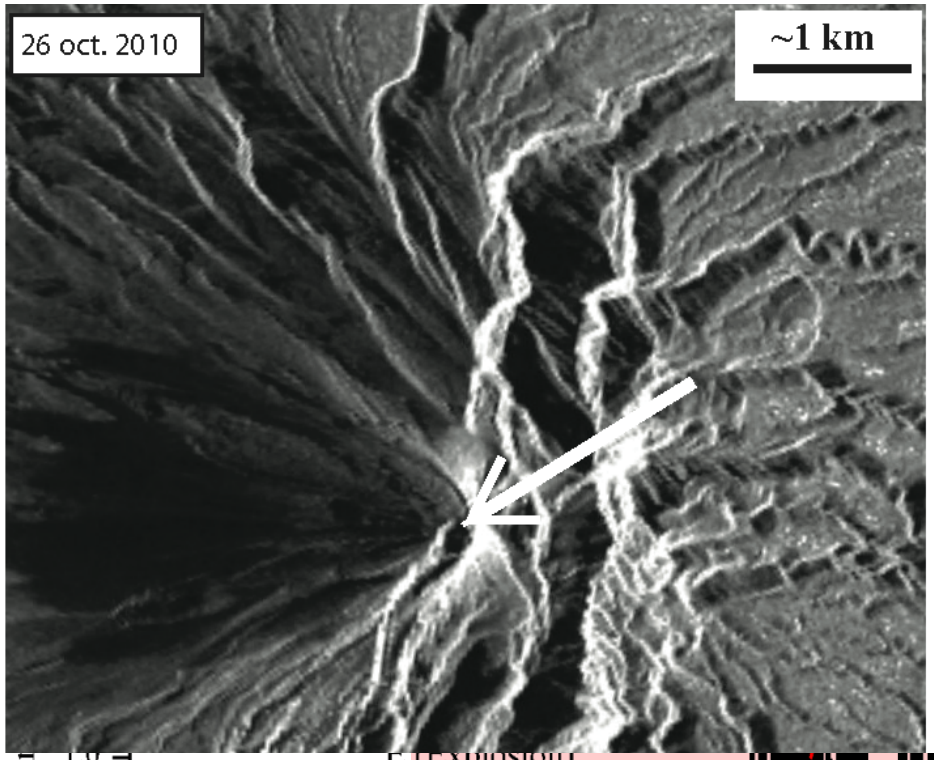

Hourly RSAM data
Cumulative RSAM data
Cumulative RSAM (x10⁸ A.U.)
Seismic A
E (Explosion)
E
E
L (Lahar)
L
L
E
L
L
L
L
L
0
0.5
1.0
1.5
2.0
20 21 22 23 24 25 26 27 28 29 30 31 01 02 03 04 05 06 07 08 09 10 11 12 13 14 15 16 17 18 19 20 21 22 23 24 25
October 2010
November 2010

Real-time Seismic Amplitude Measurement (RSAM)

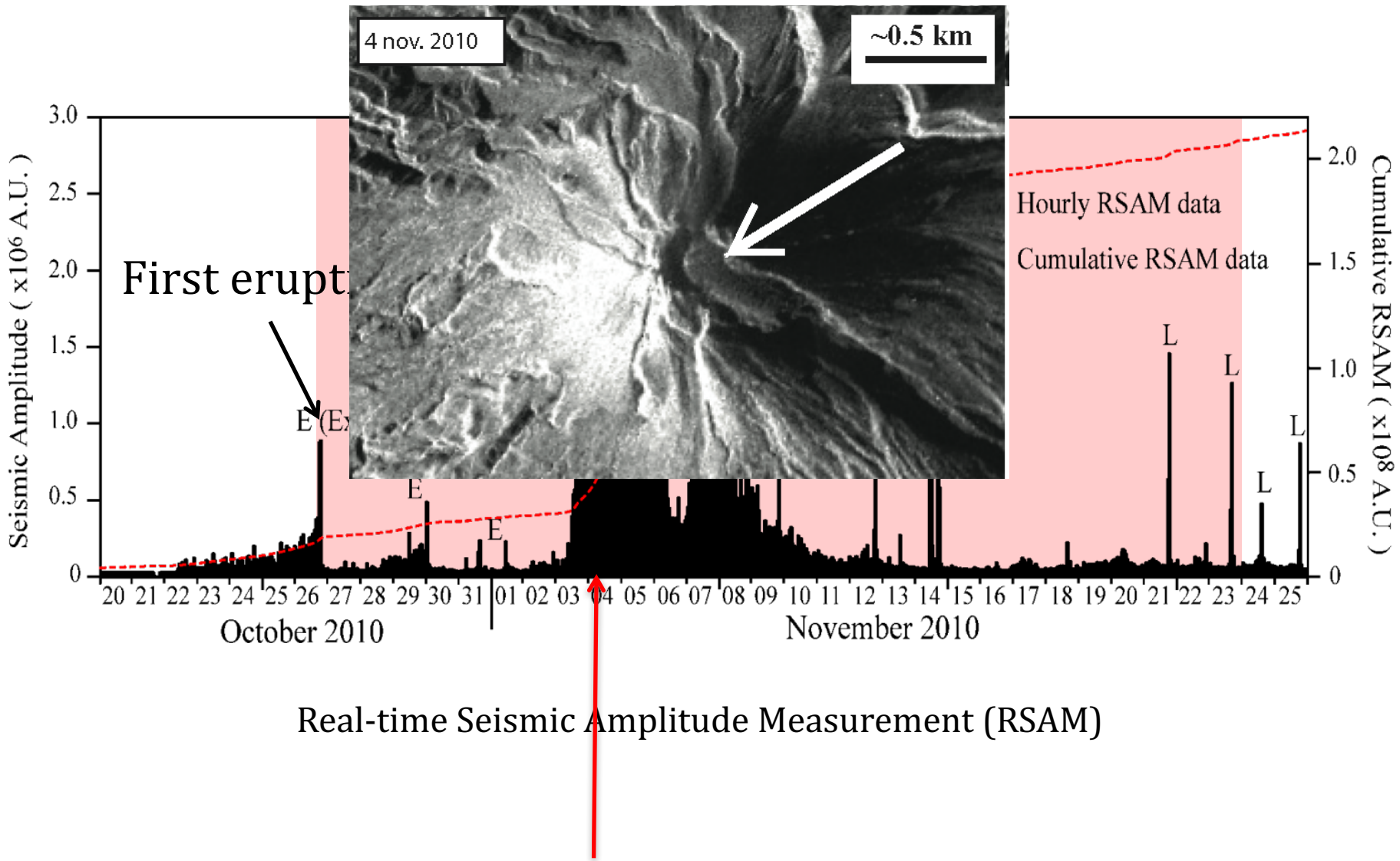

Real-time Seismic Amplitude Measurement (RSAM)

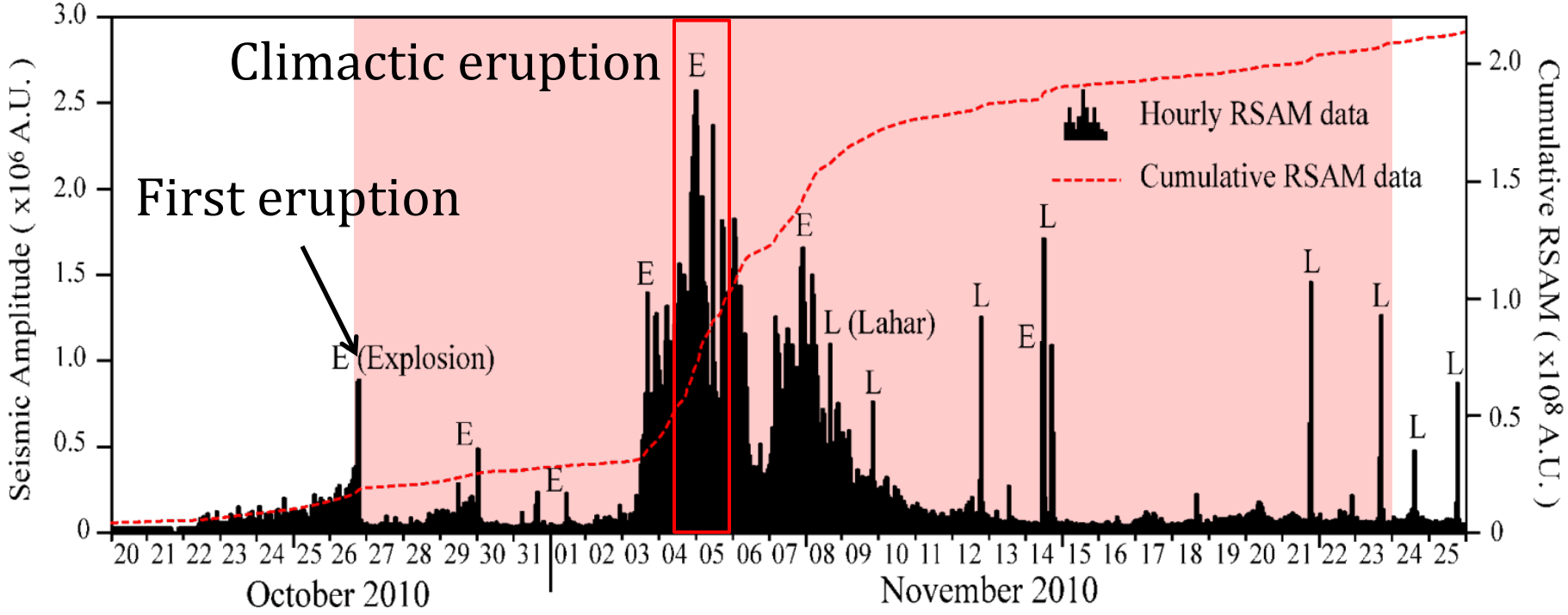

Real-time Seismic Amplitude Measurement (RSAM)

ALOS-PALSAR dataset

ALOS PALSAR:

L-band (λ = 23.62 cm)

Ascending
Track 431
Incidence angle = 34.3°
Fine **B**eam **S**ingle polarization (HH)
Fine **B**eam **D**ual polarization (HH + HV)
Resolution: 28.4 m in azimuth; 33.2 m in ground range (multilooks)

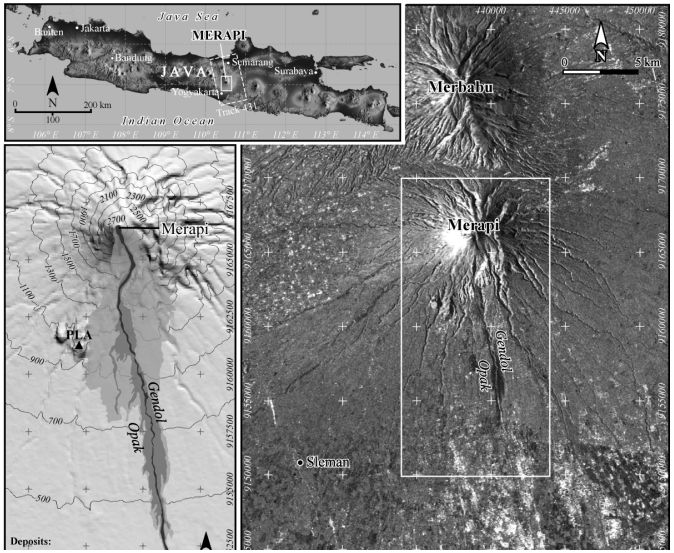

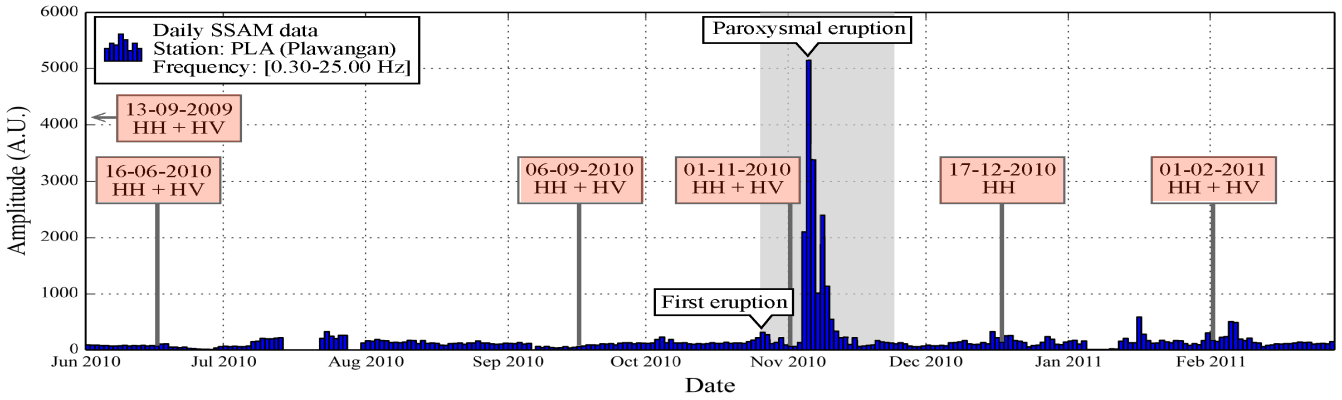

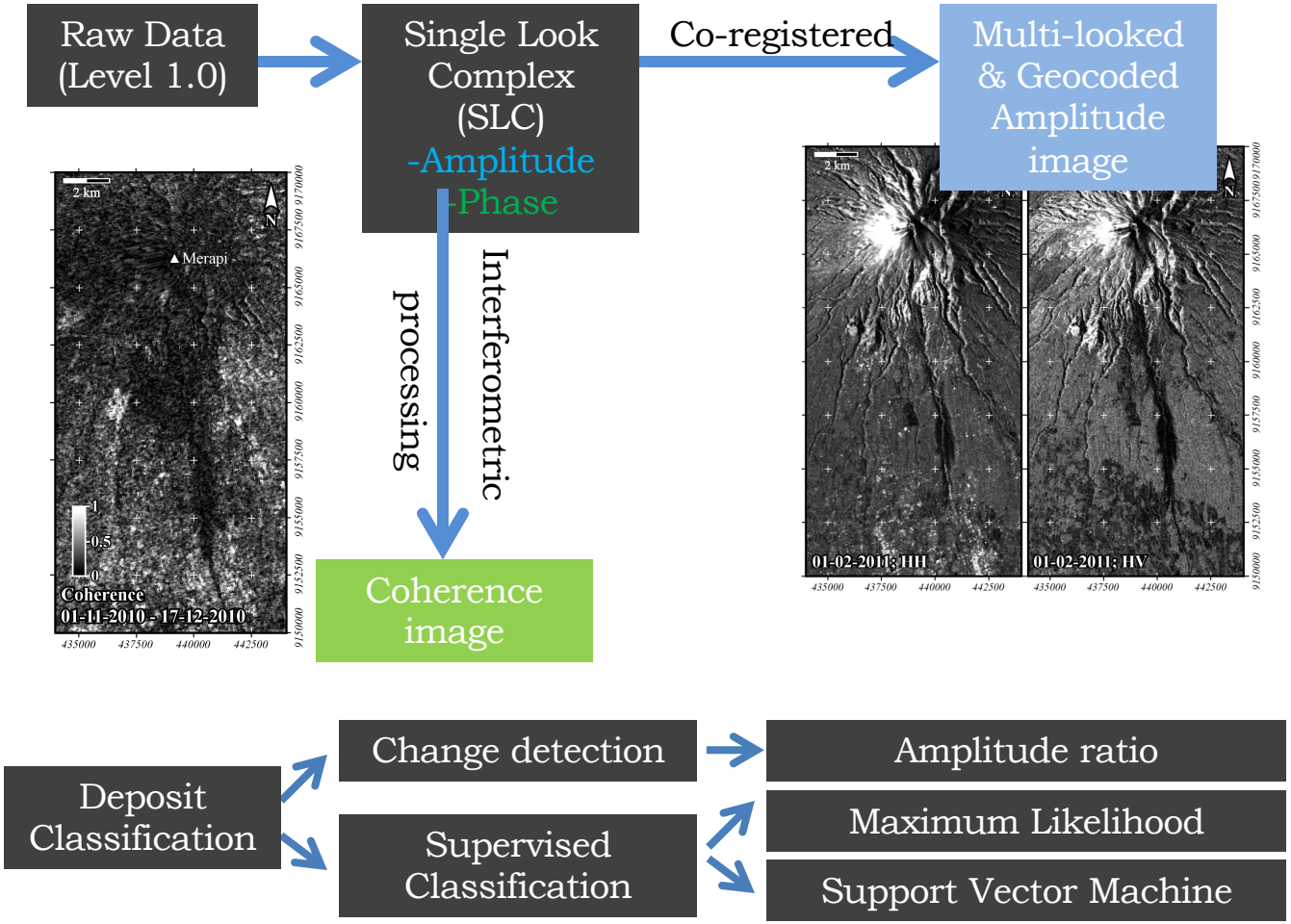
Raw Data
(Level 1.0)
Single Look
Complex
(SLC)
-Amplitude
-Phase
Co-registered
Multi-looked
& Geocoded
Amplitude
image
Interferometric
processing
Coherence
image
2 km
N
Merapi
1
0.5
0
Coherence
01-11-2010 - 17-12-2010
435000
437500
440000
442500
9170000
9167500
9165000
9162500
9160000
9157500
9155000
9152500
9150000
01-02-2011; HH
01-02-2011; HV
Deposit
Classification
Change detection
Supervised
Classification
Amplitude ratio
Maximum Likelihood
Support Vector Machine

SAR data change detection ➔ Image of amplitude ratio

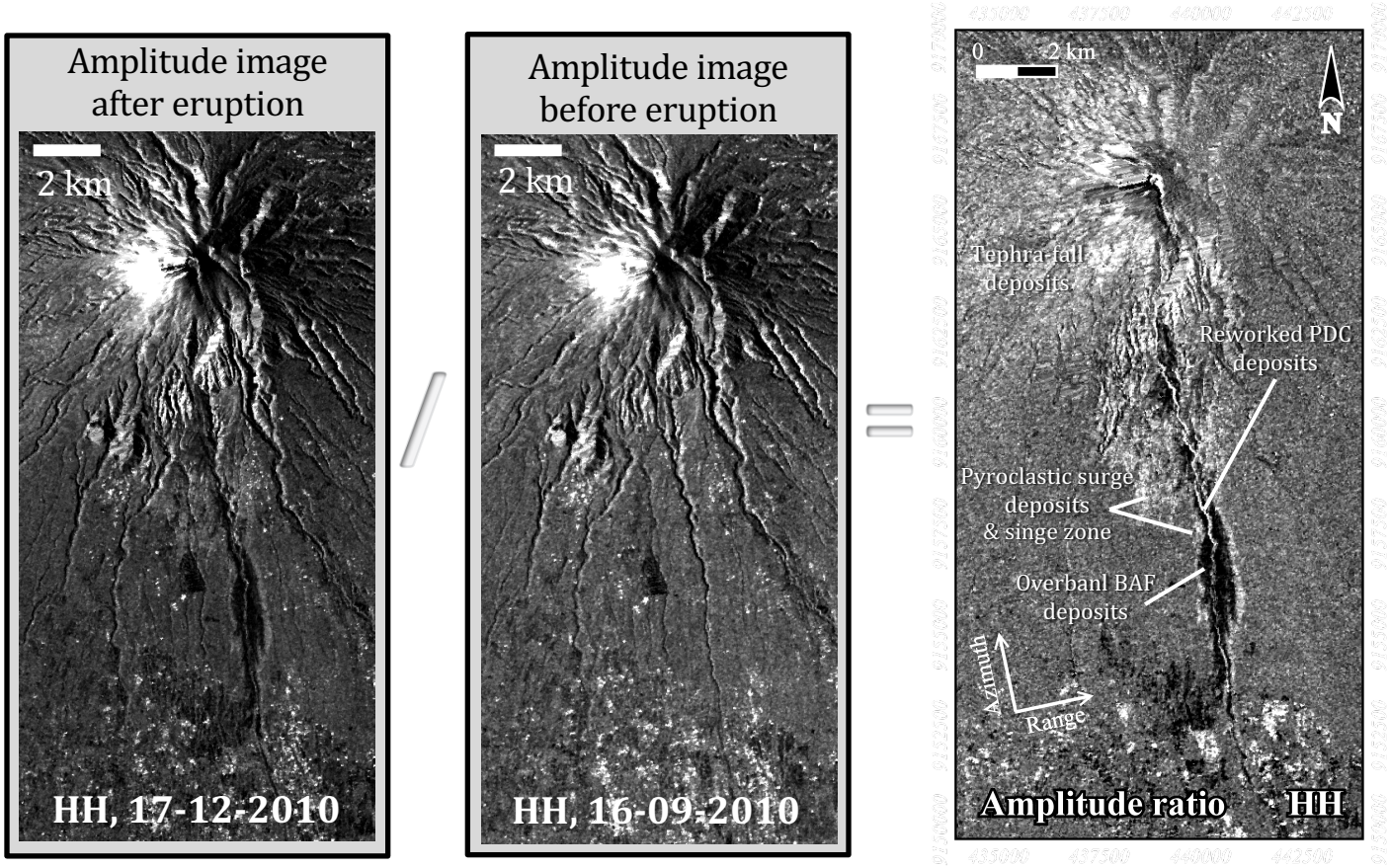

SAR data change detection ➔ False color composite image

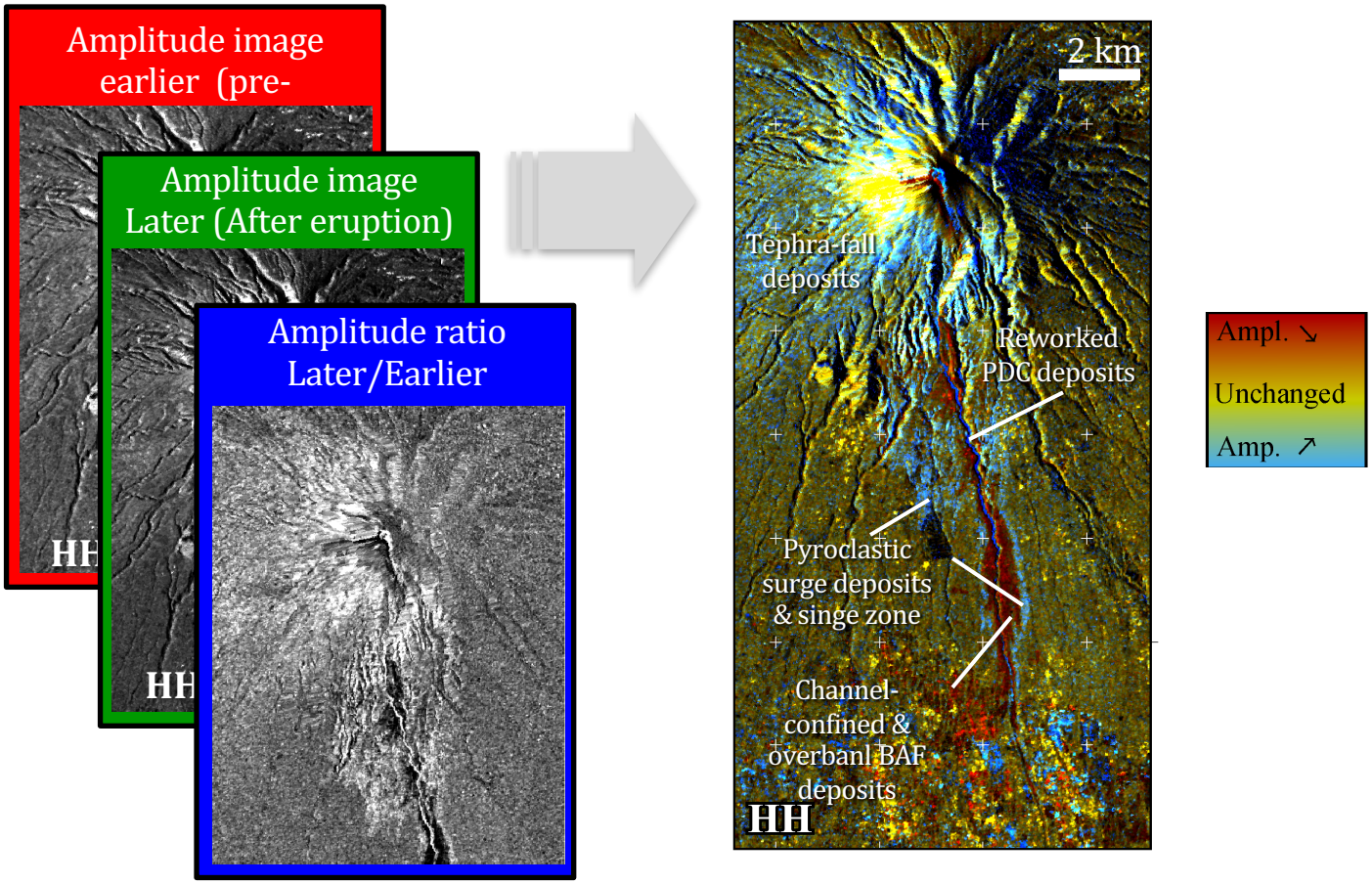

SAR data change detection ➔ False color composite image

Red: earlier Image

Green: later image

Blue: Amplitude ratio (later/ earlier)

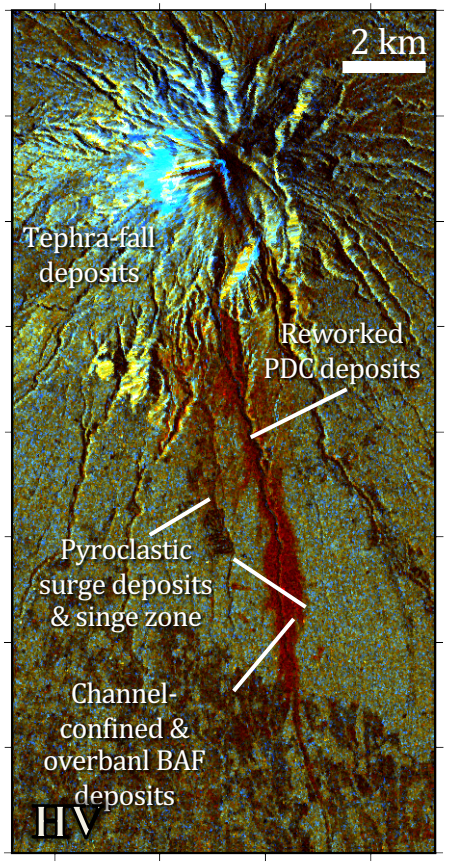

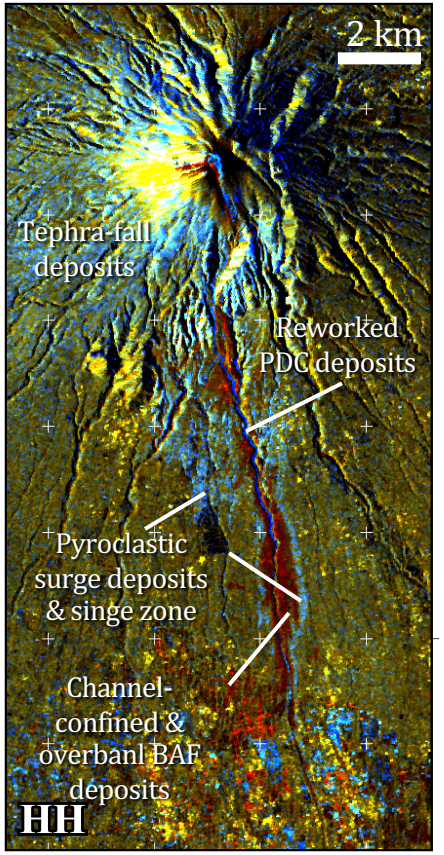

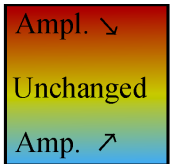

Supervised Classification

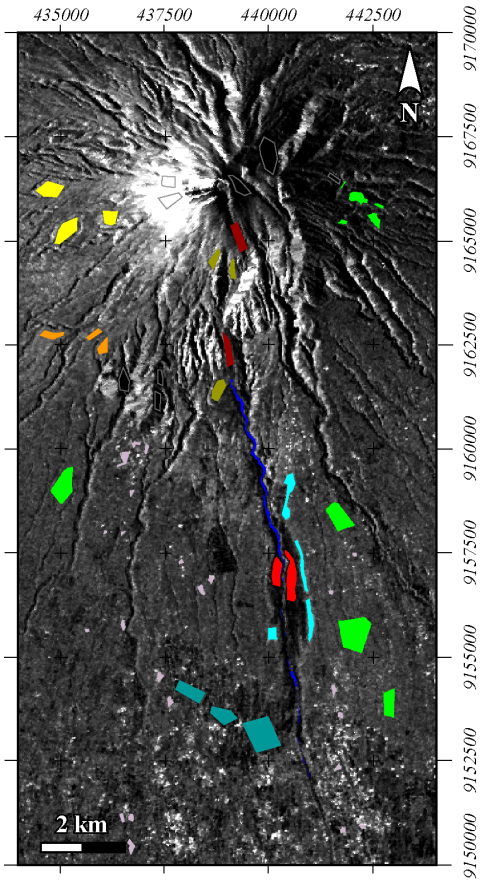

Deposits

- D1: Channel-confined and overbank BAF deposits
- D2: Reworked PDC deposits
- D3: Pyroclastic surge deposits
- D4: Tephra-fall deposits
- D5: Early stage channel-confined and overbank BAF deposits
- D6: Early stage pyroclastic surge deposits
- D7: Early stage tephra-fall deposits

Other classes

- O1: Vegetation
- O2: Agriculture / Farm
- O3: Settlements / Villages
- O4: Foreshortening effect
- O5: Shadowed area

Training Area

Supervised Classification

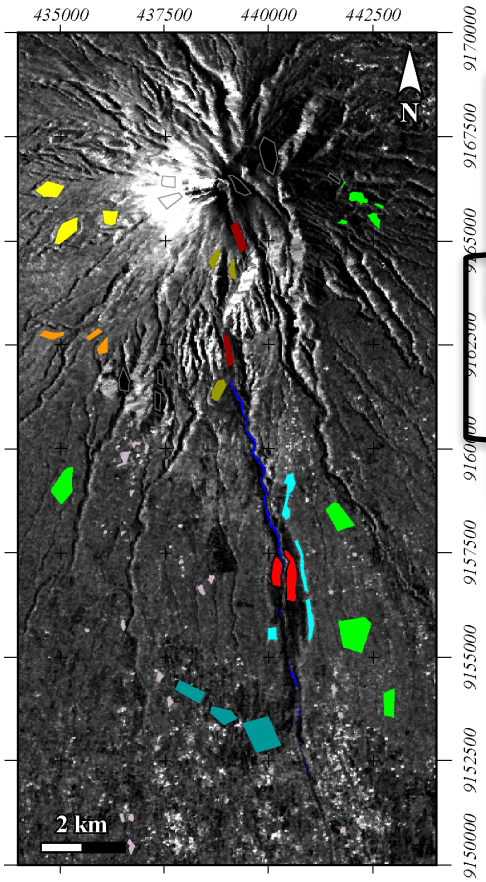

Deposits

- D1: Channel-confined and overbank BAF deposits
- D2: Reworked PDC deposits
- D3: Pyroclastic surge deposits
- D4: Tephra-fall deposits
- D5: Early stage channel-confined and overbank BAF deposits
- D6: Early stage pyroclastic surge deposits
- D7: Early stage tephra-fall deposits

Other classes

- O1: Vegetation
- O2: Agriculture / Farm
- O3: Settlements / Villages
- O4: Foreshortening effect
- O5: Shadowed area

Training Area

SAR : amplitude evolution

- **D1:** Channel-confined and overbank BAF deposits
- **D2:** Reworked PDC deposits
- **D3:** Pyroclastic surge deposits
- **D4:** Tephra-fall deposits

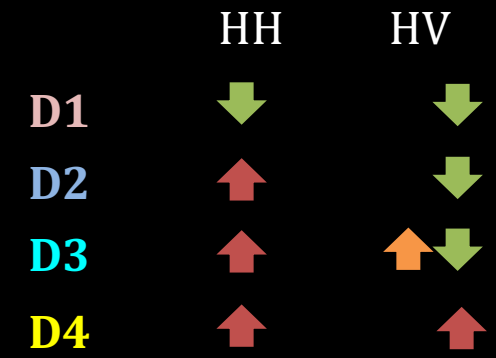

Training area

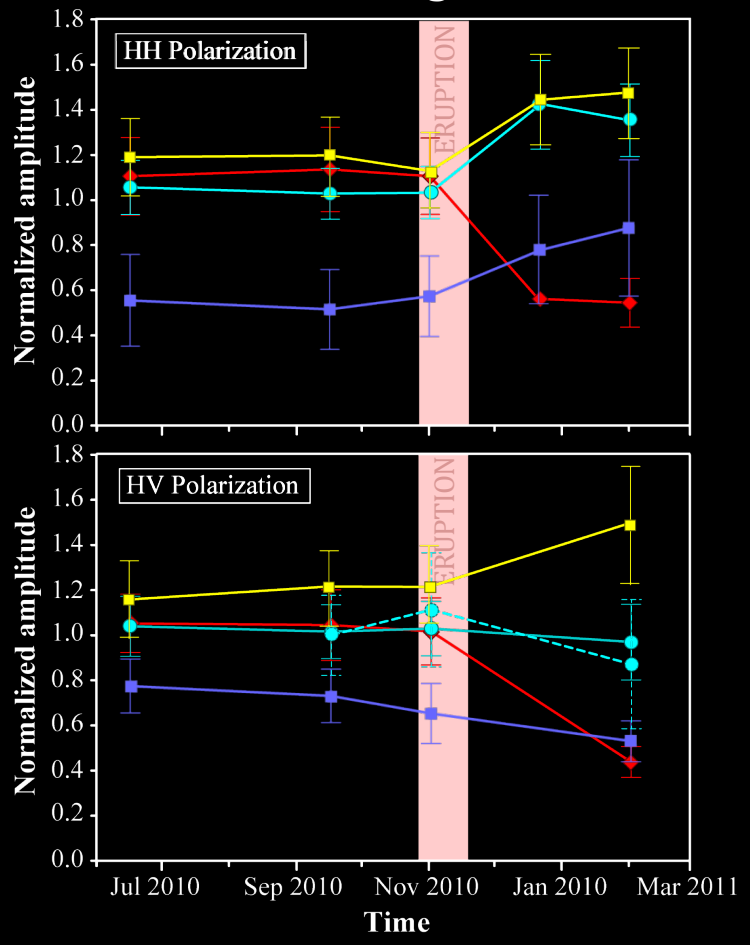

SAR : amplitude evolution

- **D1:** Channel-confined and overbank BAF deposits
- **D2:** Reworked PDC deposits
- **D3:** Pyroclastic surge deposits
- **D4:** Tephra-fall deposits

	HH	HV
D1	↓ 6.4dB	↓ 7.5dB
D2	↑ 4.6dB	↓ 2.8dB
D3	↑ 2.4dB	↑↓ <1dB
D4	↑ 2dB	↑ 1.7dB

Training area

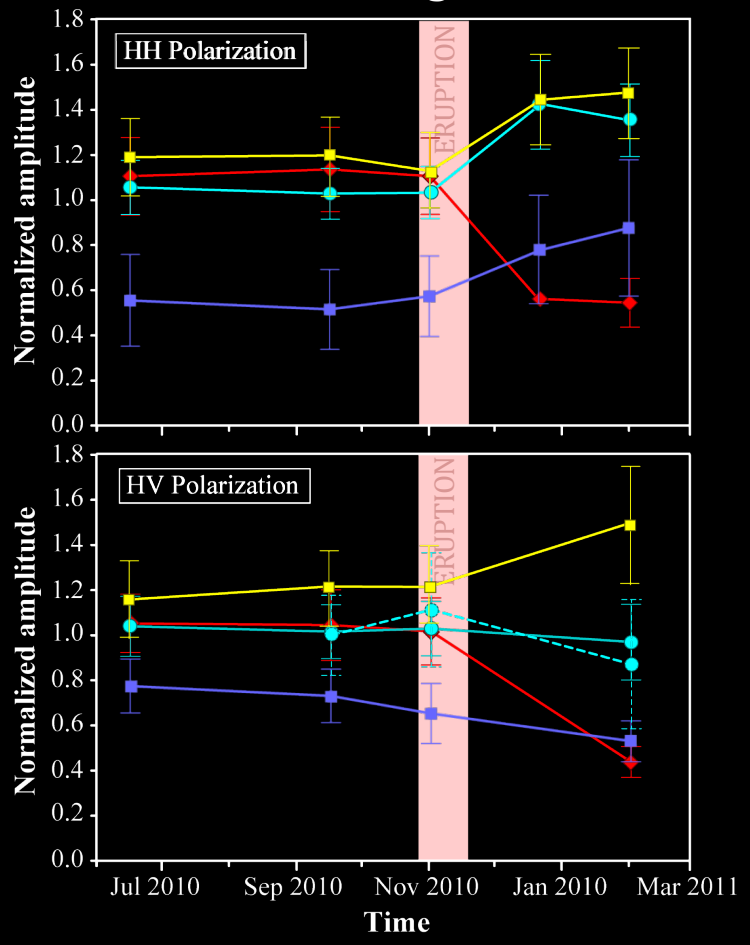

Deposit mapping

SAR : Supervised classification

- **D1:** Channel-confined and overbank BAF deposits
- **D2:** Reworked PDC deposits
- **D3:** Pyroclastic surge deposits
- **D4:** Tephra-fall deposits

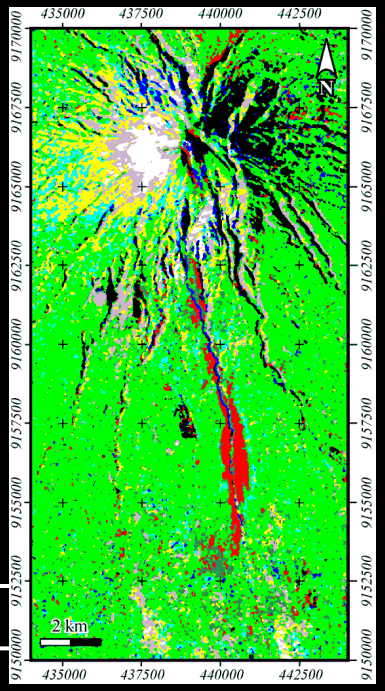

Class separability (Jeffries-Matusita distance)

Input	Separability	Pair of class
Pre-eruption HH Post-eruption HH	High	D1-D2 ; D1-D3 ; D1-D4
	Moderate	D2-D3 ; D2-D4
	Low	-
	Poor	D3-D4

High : 1.9 – 2.0 *Moderate : 1.5 – 1.9*
Low : 1.0 – 1.5 *Poor : < 1.0*

Deposit mapping

SAR : Supervised classification

- **D1:** Channel-confined and overbank BAF deposits
- **D2:** Reworked PDC deposits
- **D3:** Pyroclastic surge deposits
- **D4:** Tephra-fall deposits

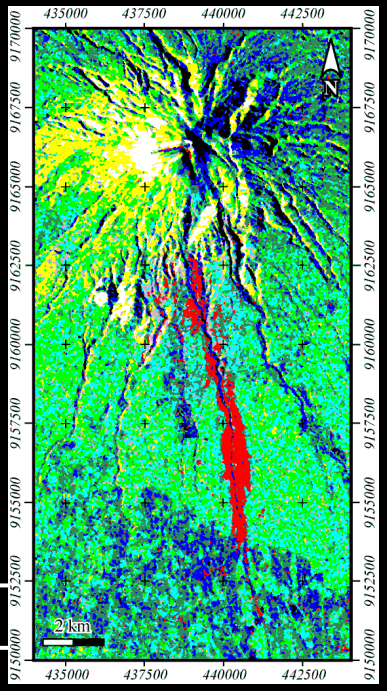

Class separability (Jeffries-Matusita distance)

Input	Separability	Pair of class
Pre-eruption HV Post-eruption HV	High	D1-D4 ; D2-D4
	Moderate	D1-D3 ; D2-D3
	Low	D1-D2 ; D3-D4
	Poor	-

High : 1.9 – 2.0 *Moderate : 1.5 – 1.9*
Low : 1.0 – 1.5 *Poor : < 1.0*

Deposit mapping

SAR : Supervised classification

- **D1:** Channel-confined and overbank BAF deposits
- **D2:** Reworked PDC deposits
- **D3:** Pyroclastic surge deposits
- **D4:** Tephra-fall deposits

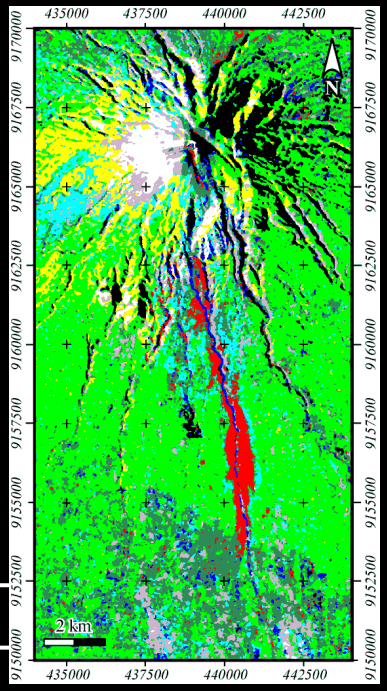

Class separability (Jeffries-Matusita distance)

Input	Separability	Pair of class
Pre-eruption HH Post-eruption HH Pre-eruption HV Post-eruption HV	High	D1-D2 ; D1-D3 ; D1-D4 ; D2-D3 ; D2-D4
	Moderate	-
	Low	D3-D4 **(1.139)**
	Poor	-

High : 1.9 – 2.0 *Moderate : 1.5 – 1.9*
Low : 1.0 – 1.5 *Poor : < 1.0*

Deposit mapping

SAR : Supervised classification

- **D1:** Channel-confined and overbank BAF deposits
- **D2:** Reworked PDC deposits
- **D3:** Pyroclastic surge deposits
- **D4:** Tephra-fall deposits

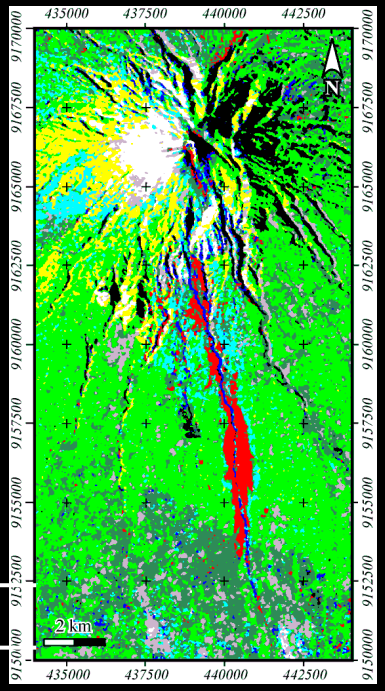

Class separability (Jeffries-Matusita distance)

Input	Separability	Pair of class
Pre-eruption HH	High	D1-D2 ; D1-D3 ; D1-D4 ; D2-D3 ; D2-D4
Post-eruption HH	Moderate	-
Pre-eruption HV		
Post-eruption HV	Low	D3-D4 **(1.227)**
Coherence image	Poor	-

High : 1.9 – 2.0 *Moderate : 1.5 – 1.9*
Low : 1.0 – 1.5 *Poor : < 1.0*

Cross-validated confusion matrix

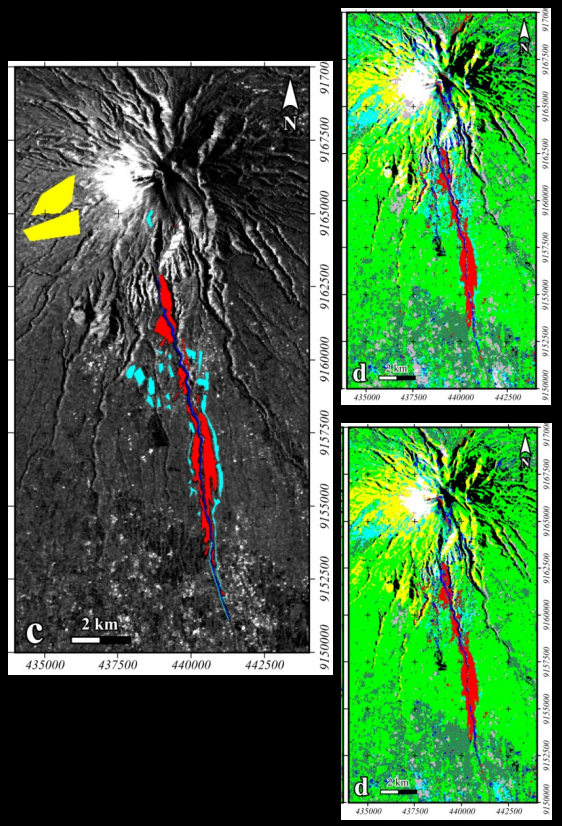

Classification Method	Classified class	Control Data (%) D1	D2	D3	D4
MLC Overall accuracy: 70.03%	D1	**86.43**	10.38	1.87	0.13
	D2	1.79	**76.77**	1.87	0.40
	D3	1.62	3.42	**58.48**	30.61
	D4	0.00	0.12	2.85	**55.47**
SVM Overall accuracy: 63.97%	D1	**89.83**	8.49	2.55	0.08
	D2	2.39	**74.41**	2.51	0.35
	D3	0.15	2.12	**27.29**	24.66
	D4	0.00	0.00	4.11	**54.67**

TerraSAR-X dataset

X-band (λ = 3.1 cm)
Descending
Track 134
Incidence angle = 37.4°
Single polarization (HH)
Resolution: 8.9 m in azimuth;
5.5 m in ground range (multilooks)

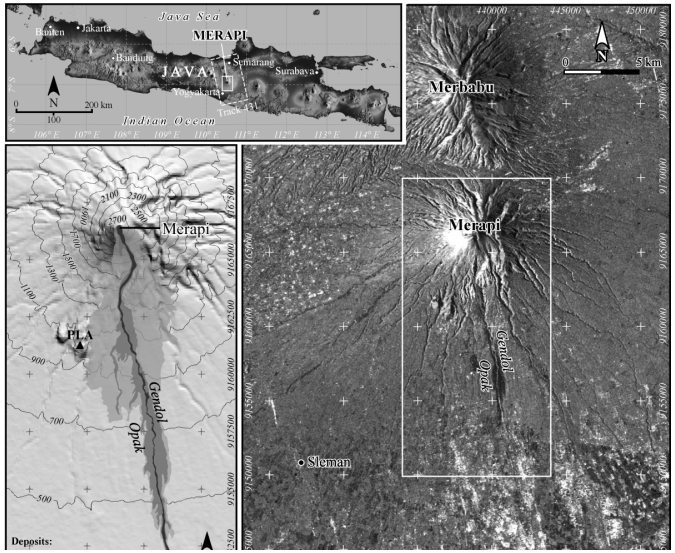

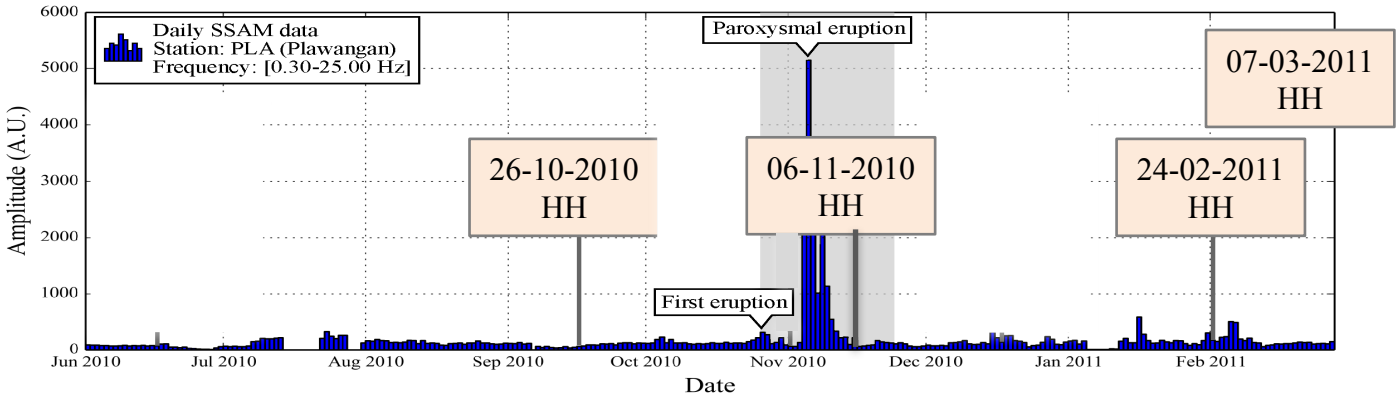

TerraSAR-X on the 2010 Merapi eruption

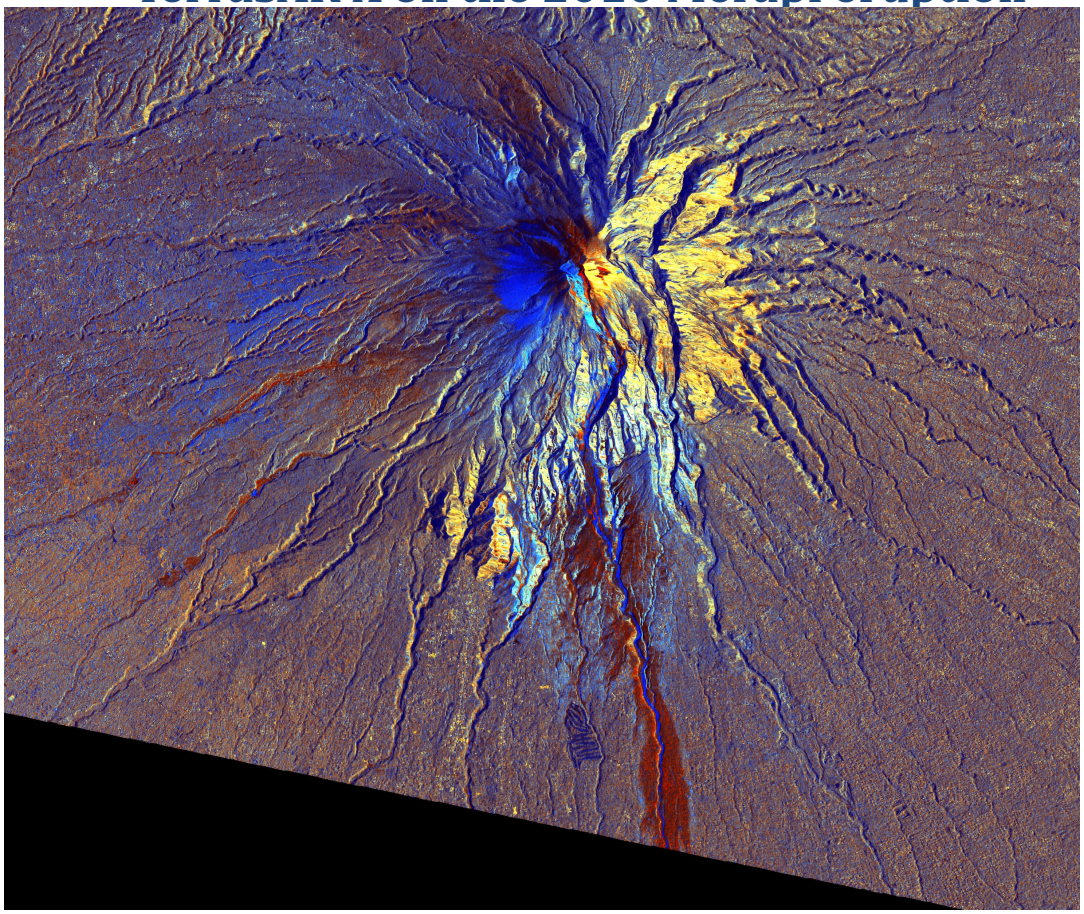

R: 26-10-2010 G: 06-11-2010 B: ratio (06-11-2010/26-10-2010)

TerraSAR-X on the 2010 Merapi eruption

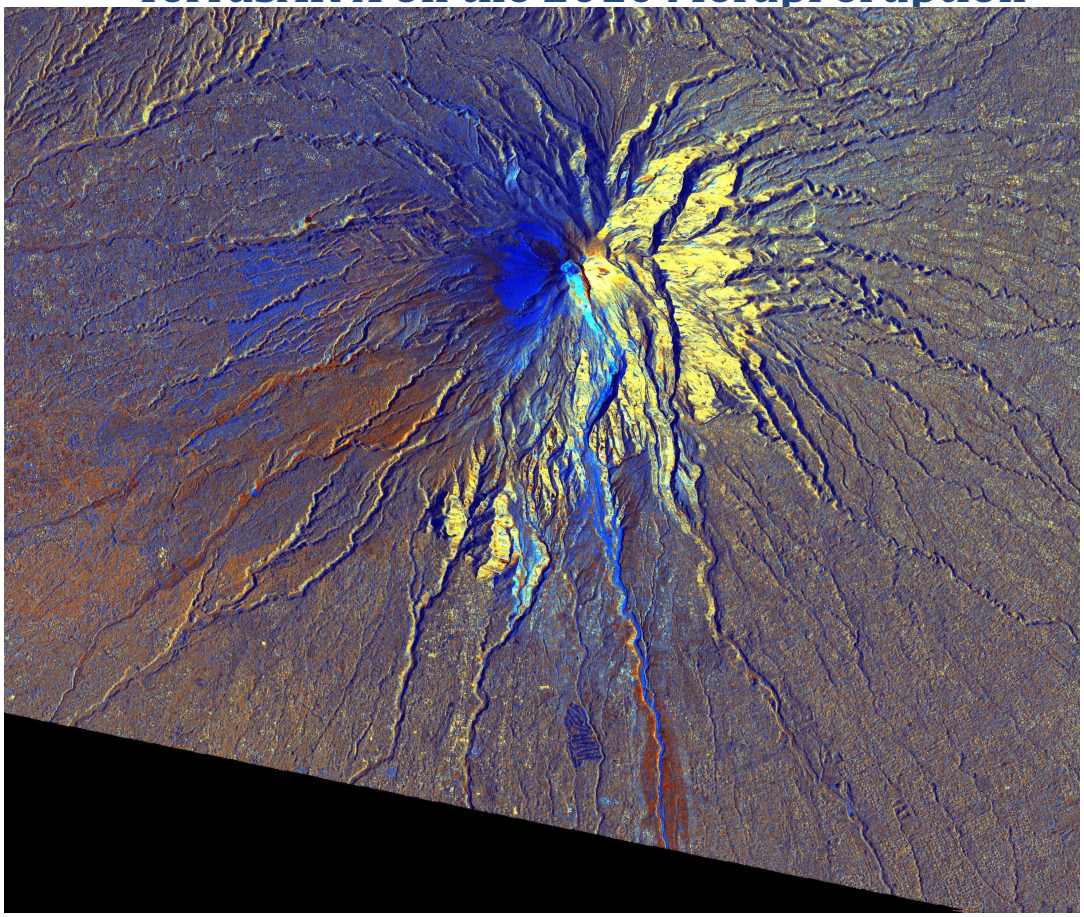

R: 26-10-2010 **G: 24-02-2011** **B: ratio (24-02-2011/26-10-2010)**

TerraSAR-X on the 2010 Merapi eruption

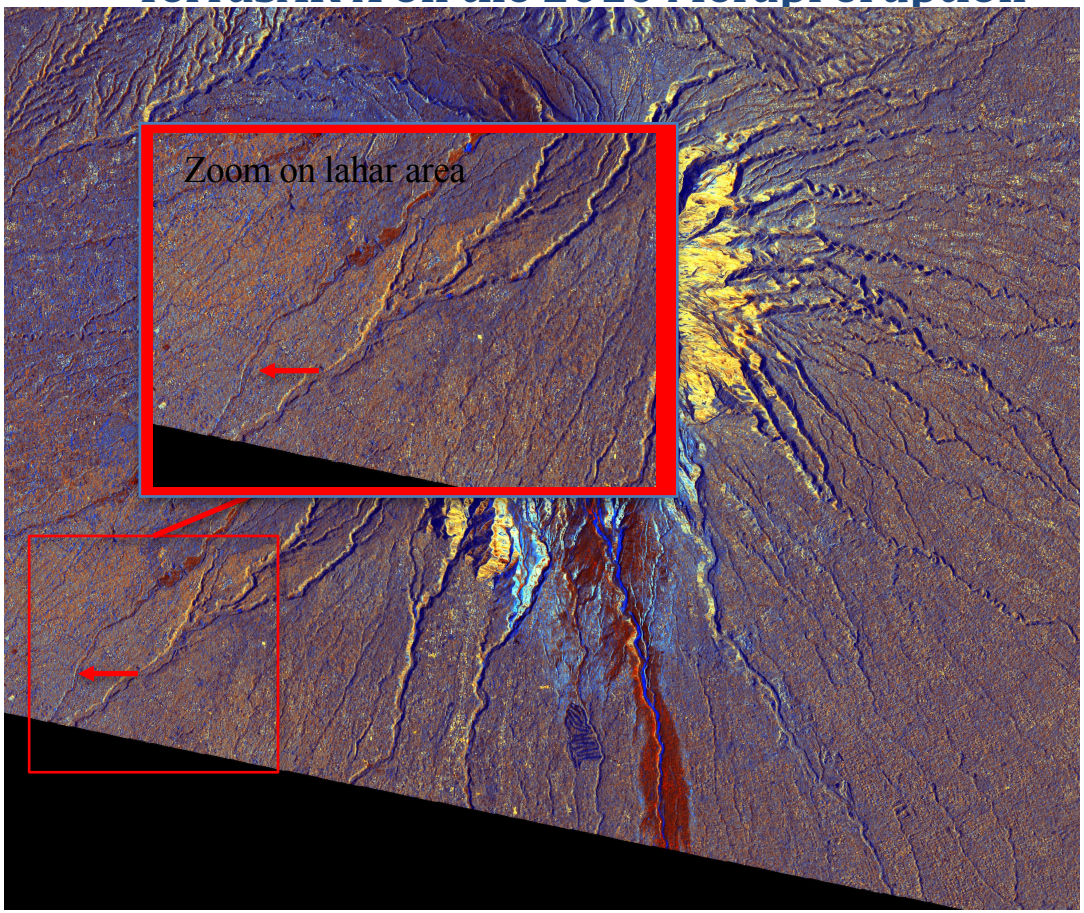

R: 26-10-2010 **G: 06-11-2010** **B: ratio (06-11-2010/26-10-2010)**

TerraSAR-X on the 2010 Merapi eruption

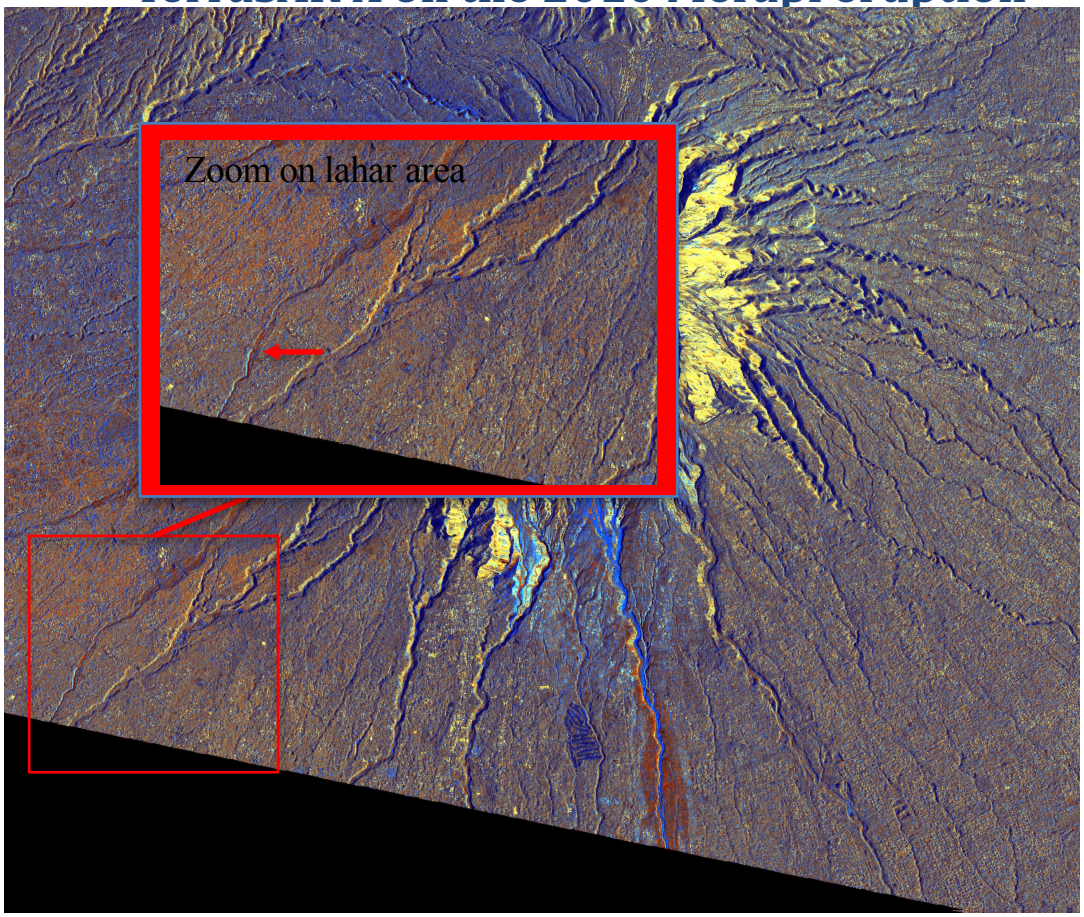

R: 26-10-2010 **G: 24-02-2011** **B: ratio (24-02-2011/26-10-2010)**

TerraSAR-X on the 2010 Merapi eruption

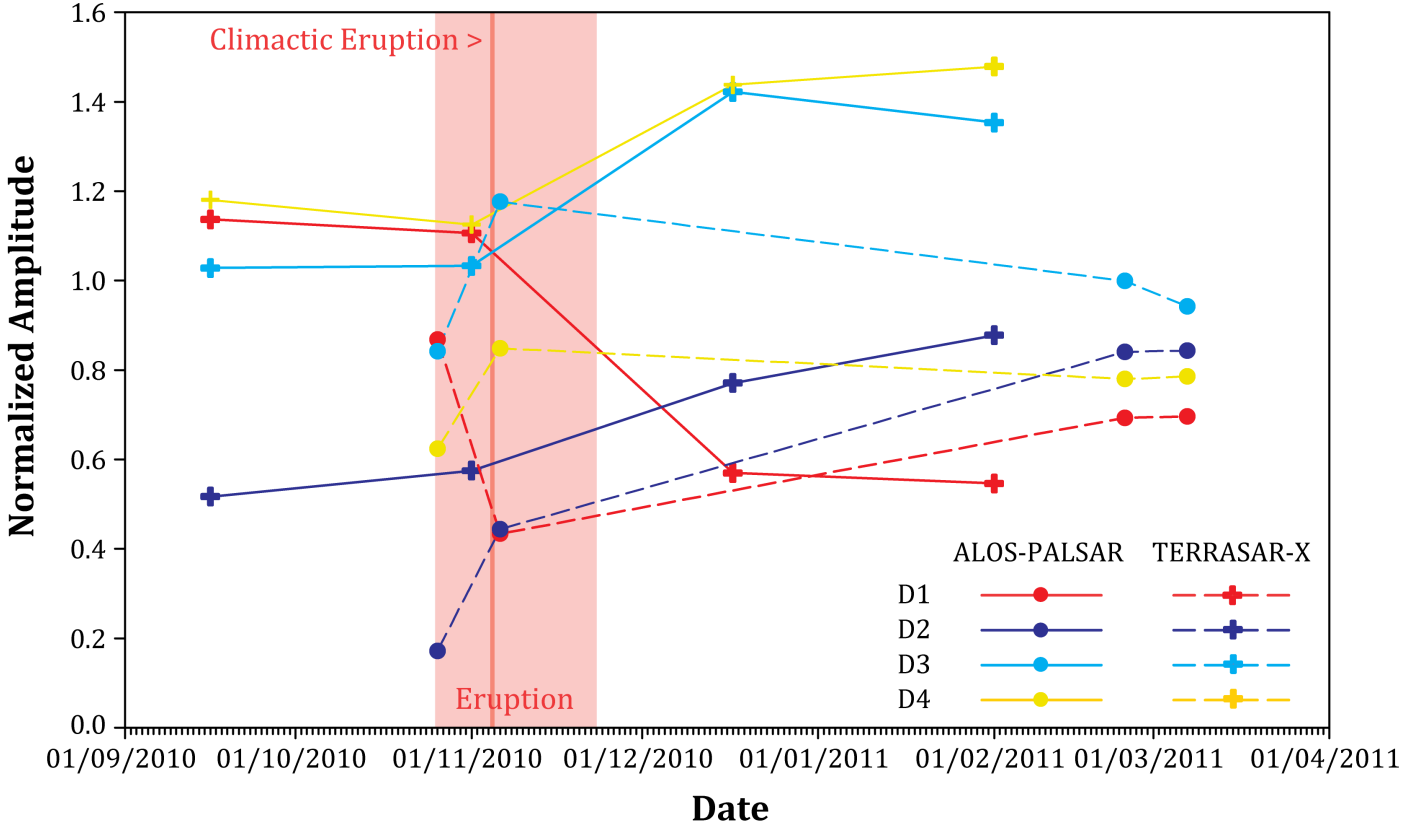

Conclusions on Merapi study

- Classification is improved when combining phase and amplitude information and using polarized data
- Surface estimations:

  D1 + D2 : 6.66 km² (6.53 km² by optical imagery *from Charbonnier et al, 2013*)

  D3 : 5 km² (15.77 km² by optical imagery *from Charbonnier et al, 2013*)

- Similar behaviour for L and X-band on HH data

Example of information: Detection/quantification of summit structural changes by SAR

TerraSAR-X data: X-band (λ = 3.1 cm), ascending track 96, spatial resolution 3*3m

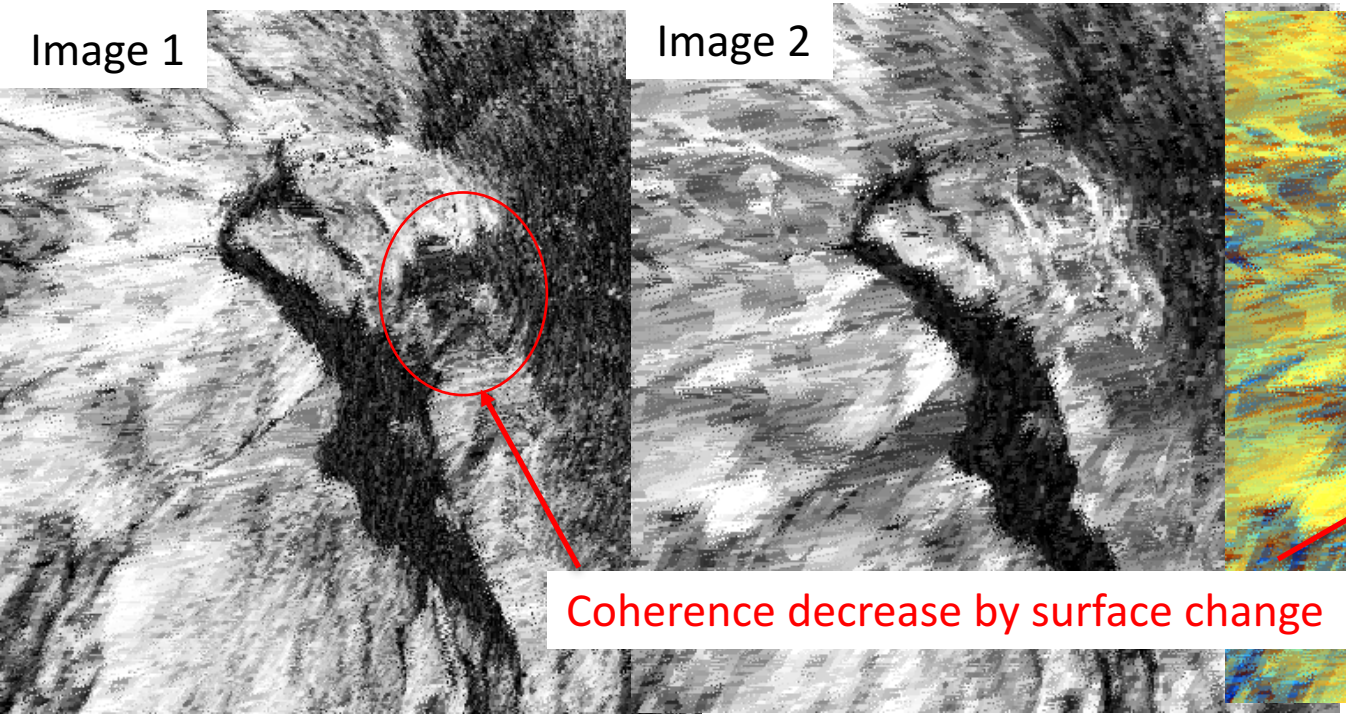

Coherence image (co-event)
20141231-20150111

Coherence image (post-event)
20150111-20150122(reference)

RGB: R: image 1; G: image2
B:image2/image1

Bibliography

*Massonnet, D., Feigl, K.L., 1998. Radar interferometry and its application to changes in the Earth's surface. Rev. Geophys. 36, 441–500.
*Massonnet, D., Sigmundsson, F., 2000. Remote sensing of volcano deformation by radar interferometry from various satellites. Remote Sensing of Active Volcanism vol. 116. AGU, Washington, DC, pp. 207–221
*Zebker, H., Amelung, F., Jonsson, S., 2000. Remote sensing of volcano surface and internal processes using radar interferometry. In: Mouginis-Mark, P.J., Crisp, J.A., Finks, J.H. (Eds.), Remote Sensing of Active Volcanism vol. 116. AGU, Washington, DC, pp. 179–205.
* M. Simons and P. Rosen, Treatise on Geophysics, Interferometric Synthetic Aperture Radar Geodesy, Schubert, G. (ed.), Volume 3- Geodesy, Elsevier Press, pp. 391-446, 2007
*V. Pinel, M. Poland, A. Hooper, Volcanology : Lessons learned from Synthetic Aperture Radar imagery, *J. Volcanol. Geotherm. Res.,* 81-113, 10.1016/j.jvolgeores.2014.10.010, 2014.

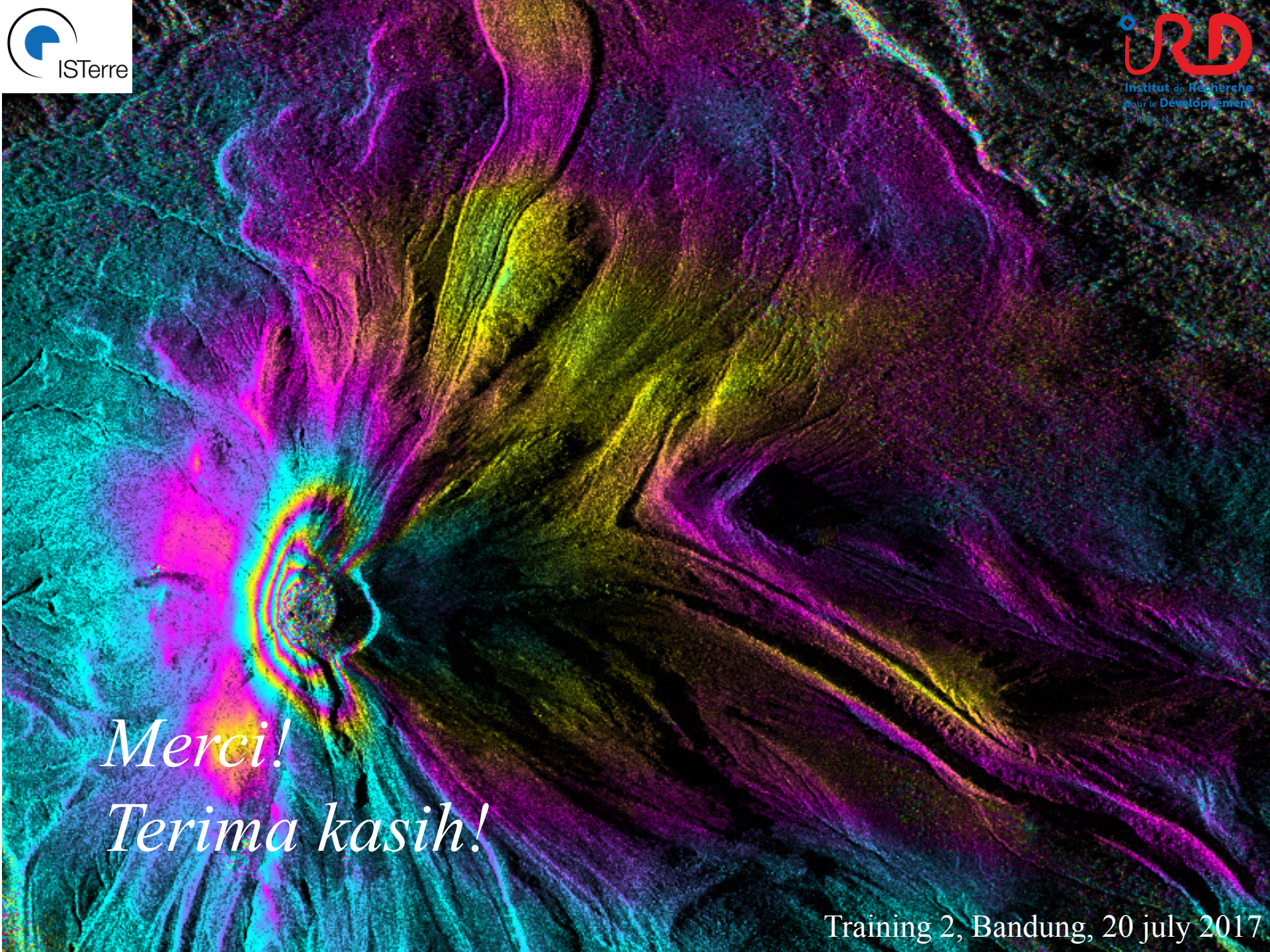
ISTerre
Institut de Recherche pour le Développement
FRANCE
Merci!
Terima kasih!
Training 2, Bandung, 20 july 2017